# First tomographic observations of gravity waves by the infrared limb imager GLORIA

Isabell Krisch et al.

October 26, 2017

Dear Editor, Dear Reviewers,

Thank you very much for these very helpful comments!Many thanks to the Editor and also many thanks to all Referees for their very helpful comments that significantly helped to improve the manuscript! This is a short summary of the changes that are made in the revised manuscript. For more details see out point-by-point reply to all reviewer comments.
The main changes due to comments made by Reviewer #1 can be summarized as follows:

According to comment #1 we will include details on the smoothing filter used for the generation of the a-priori field as well as on the calculation of the occurrence probability (comment #3). Comment #2 is a valuable hint and we will change the determination of the resolution. Instead of the sphere in the horizontal and the FWHM of the row of the averaging kernel in the vertical, we will now use a 3D ellipsoid to estimate the resolutions in horizontal and vertical simultaneously. This new technique will account for the diagonal elements of the AVK matrix. However, applying the new method does not change the resulting resolution values. In the appendix we will clarify the sentence mentioned in comment #4.

The main changes due to comments made by Reviewer #2 can be summarized as follows:

To increase the visualization of the paper, Figures 2 and 3 will be updated according to remarks #25 and #26. According to comment #33, the physical meaning of the total momentum, which is a measure for the drag, a GW event can exert on the atmosphere, will be better explained. This number is especially important as it can be compared to the GW drag of GCMs and cannot be provided by 1D wind observations. Comment #34 has been mentioned in a similar way by all referees. We will include more details on how the occurrence probabilities were determined. A similar distribution derived from GLORIA measurements (comment #39), cannot be provided, as tomographic measurement patterns are event based only and, thus, not suitable for a statistical analysis. We very much appreciate remark #44 and will extend the discussion on the different results of 1D and 4D ray-tracing, respectively. Further we will include a paragraph on how the results of our paper can advance GW parameterizations.

The main changes due to comments made by Reviewer #2 can be summarized as follows:

According to comment #2 we will include details on the smoothing filter used for the generation of the a-priori field. Further, we will include a figure with a comparison of GLORIA and in-situ measurements (comment #4). As mentioned by the Referee, this will further support the capabilities of GLORIA. Regarding comment #5, the authors want to clarify, that for the derivation of Equation (2), the mid-frequency approximation was not used. However, the low and high frequency terms of Equation (6) in Ern et al. (2004) have been omitted in our paper, as their impact on the result is below 1% in the measured gravity wave range. This will be addressed in the revised manuscript. Comment #6 has been mentioned in a similar way by all referees. We will include more details on how the occurrence probabilities are determined. A comparison of GLORIA measurements with ECMWF shows that for the case discussed in our paper, the GWMFs have a similar magnitude. Therefore, we have confidence that the statistics derived from ECMWF are a meaningful way to set our event into a broader context.

For details and our reply to all other comments see the point-by-point reply and the revised manuscript.

Again, thank you very much for your effort!

Sincerely, Isabell Krisch

## References

Ern, M., Preusse, P., Alexander, M. J., and Warner, C. D.: Absolute values of gravity wave momentum flux derived from satellite data, Journal of Geophysical Research: Atmospheres, 109, doi:10.1029/2004JD004752, URL `http://dx.doi.org/10.1029/2004JD004752`, 2004.

# Point-by-point reply

Isabell Krisch et al.

October 26, 2017

## Reviewer #1

**Reviewer comment:** What smoothing filter was used (type and fwhm) for the a-priori field generation?
**Authors response:** More details will be included in the text.
**Text changes:** This smoothing was done by applying a low-pass Fourier filter with cut-off wavenumber 18 in zonal direction. In height and latitude direction Savitzky-Golay (SG) filter (Savitzky and Golay, 1964) was applied with 4th order polynomials over 11 and 25 neighbouring points respectively. On the one hand, the so generated a-priori field improves the convergence speed of the iterative minimization, as this temperature structure is close to the true values due to the high quality of the ECMWF model. On the other hand, the smoothening ensures that any GW signature in the retrieval result does not stem from the used a priori data. If the a-priori data exerts any influence, it would dampen the GW structure.

**Reviewer comment:** Are you simply looking at the elements in the row of the AVK matrix corresponding to the grid points directly above the grid-point of the row, or are you collapsing (i.e. performing a summation) the two other dimensions (x,y) before this FWHM is calculated? If the first approach is used, some description of the elements located diagonally above and below the grid-point should be included, as these can (in principle at least) indicate information leakage from higher altitudes that the elements directly above.
**Authors response:** The determination technique for the resolution will be changed to a 3D ellipsoidal fit to include diagonal matrix elements. However, applying the new method, does not change the resulting resolution values.
**Text changes:** The horizontal and vertical resolutions can be defined by the axes of the smallest ellipsoid containing all elements of the averaging kernel larger than half the maximum. Accordingly, in the middle of the performed hexagonal flight path, the vertical resolution is around 200 m, the horizontal resolution around 20 km.

**Reviewer comment:** How are the GW located in the ECMWF data and how are the occurrence frequencies calculated? a bit more details on how this was done would be good to include.
**Authors response:** We will include the details on how the occurrence probabilities are determined in the manuscript.
**Text changes:** To classify this event, a comparison of all GW events in January 2016 has been performed in the 6-hourly operational analyses of ECMWF. First the temperature background was isolated, as described in Sec. 2.1 for the a-priori field, and subtracted from the original field. The remaining temperature residuals were analyzed for GWs using the 3D sinusoidal fit algorithm described above. The GWMFs for all cubes were calculated. The GWMFs from all 124 analyses fields were combined to obtain the probability of GW occurrence (Fig. 6, *former Fig. 5*). Here, all GWMF values were considered independent of the horizontal and vertical wavelengths. Removing wavelengths larger than 2.5 times the cube size in order to filter less significant fits (not shown) induced no major changes in the general shape of the distribution. This indicates that GW events with less certain fits do not bias the probability distribution. For the GW event over Iceland similar GWMF magnitudes were determined from the ECMWF analyses and from the GLORIA measurements. Thus, a comparison of the measurement results with the occurrence probability determined from the ECMWF analyses seems reasonable. According to Fig. 6 the measured GW event can be classified as a very strong case since the sum of all occurrence probabilities of stronger events is far below 1%.

**Reviewer comment:** What is meant by full height range of the S3D fitting volume? Does it refer to each individual fitting volume i.e. 160 km x 160 km x 3.6 km?
**Authors response:** The sentence will be restructured to clarify this point.
**Text changes:** In Fig. A1 left column the instantaneous value $\xi_{z=11.5}$ of the ray at the middle point of each fitting volume is compared to an average $\bar{\xi}$ of all values of the ray in the height range of the respective S3D fitting volume (comparable to the S3D fitting result).

## Reviewer #2

**Reviewer comment:** Page 1, Line 2-3, the term global atmospheric circulation models. Even there are more than one options, mostly GCM refers to general circulation model.
**Authors response:** All occurrences of global atmospheric circulation models will be replaced by general circulation model.

**Reviewer comment:** Page 1, Line 5, measured - observed/revealed.
**Authors response:** This will be changed in the manuscript.

**Reviewer comment:** Page 1, Line 12-13, the last sentence should be reworded.
**Authors response:** The last sentence of the abstract will be reworded.
**Text changes:** Forward ray-tracing reveals that the waves propagate laterally more than 2000 km away from their source region. A comparison of a 3D ray-tracing version to solely column based propagation showed that lateral propagation can help the waves to avoid critical layers and propagate to higher altitudes. Thus, the implementation of oblique gravity wave propagation into general circulation models may improve their predictive skills.

**Reviewer comment:** Page 1, Line 17, I do not see a good logic relation when using Thereby.
**Authors response:** The relation between the two sentences will be clarified.
**Text changes:** The exerted drag induces the meridional circulation in the mesosphere / lower thermosphere (MLT) and finally leads to the cold summer mesopause and the warm winter stratopause.

**Reviewer comment:** Page 1, Line 20, add abbreviation QBO for quasi-biennial oscillation.
**Authors response:** The abbreviation will be added.

**Reviewer comment:** Page 2, Line 14, there are more published papers about the gravity wave parameterization schemes such as Alexander and Dunkerton 1999, Beres et al. 2004 and 2005, Richter et al. 2010. Page 2, Line 15, besides the source distribution, the launched wave propagation direction is another simplification.
**Authors response:** A more detailed list of references on GW parameterization schemes will be included. The simplifications in the source distributions have been mentioned.

**Reviewer comment:** Page 2, Line 24, polarization - polarisation, analyzed - analysed, you may skip this since they are just differences between American and Bristish English.
**Authors response:** This will be addressed in the revised manuscript.

**Reviewer comment:** Page 2, Line 25, there are several published papers using multiple instruments (colocated or network) to study the 3D strucuture of gravity waves such as Lu et al. 2016 (two lidar and imager), Cao et al. 2016 (lidar and imager), Bossert et al. 2015 (lidar and imager).
**Authors response:** The mentioned further examples of 3D measurements in the mesosphere have been mentioned in the manuscript. However, these measurements have the same restriction as the MAARSY measurements, that they are far away from the sources and limited to few ground based stations.
**Text changes:** In the mesosphere, a full wave characterization of short scale GWs has been achieved with the Middle Atmosphere Alomar Radar System (MAARSY; Stober et al., 2013). For medium scale GWs in the mesosphere, a full characterization has been derived by combining lidar and airglow imager measurements (Bossert et al., 2015; Lu et al., 2015; Cao et al., 2016). However, all these observations are limited to a few ground based stations. Further, it is difficult to link observations at altitudes as high as the mesopause region to specific GW sources, which are usually located at much lower altitudes in the troposphere and lower stratosphere. So far no measurement technique existed to measure the 3D structure of mesoscale GWs in the lower stratosphere.

**Reviewer comment:** Page 3, Line 5, remove measurement
**Authors response:** This word will be removed.

**Reviewer comment:** Page 3, Line 7, the title of this section could better be Data and Methodolody. Page 7, Section 3 title Analysis-Results.
**Authors response:** Both section titles will be changed.

**Reviewer comment:** Page 3, Line 18, I suppose less pixels are used thus the readout time is reduced.
**Authors response:** This will be addressed in the text.

**Reviewer comment:** Page 3, Line 23, what is the aircraft flight altitude? what is the altitude range the measurements are taken?
**Authors response:** These points will be included in the manuscript.
**Text changes:** The aircraft flight altitude during this time was between 12.5 km and 13.5 km. Towards low altitudes, the GLORIA measurements were limited by clouds reaching up as far as 9 km to 10.5 km.

**Reviewer comment:** Page 4, table 1 caption, the second sentence: The last column indicates the retrieved quantity for each spectral range.
**Authors response:** This will be changed in the text.

**Reviewer comment:** Page 4, Line 12, this part - which part? the altitude range?
**Authors response:** This will be changed in the text.

**Reviewer comment:** Page 5, Line 7, what is the temporal resolution, such as the integration time or exposure

time?
**Authors response:** A sentence on the temporal resolution will be added to Sec. 2.1.
**Text changes:** The time needed to accomplish the hexagon was about 2 h. During this time 2200 infrared images and corresponding spectra were taken. The presented tomographic retrieval represents a temporal mean over all these measurements.

**Reviewer comment:** Page 5, Line 9-10, what is the evidence that this is a mountain wave? This is important because this is the prerequisite of fitting. Is it stationary or near stationary during your 2 hour observation window?
**Authors response:** These waves were predicted by the ECMWF forecast to be stationary above Iceland for more than 6 hours. This will be included in the text.

**Reviewer comment:** Page 5, Line 12, remove as discussed in Sec. 3.2. It is not proper to refer to something in latter discussions.
**Authors response:** This will be removed.

**Reviewer comment:** Page 5, Line 17, GW-GWs.
**Authors response:** This will be changed.

**Reviewer comment:** Page 5, Line 18-19, what is the relation between S-G filter and the polynomial fitting?
**Authors response:** The method proposed by (Savitzky and Golay, 1964), which is called Savitzky-Golay filter, is based on a so-called running polynomial fitting. A polynomial of order k is fitted to a box of n neighbouring points and the middle point is replaced by the value of the fit. This is done for all data points by shifting the boxes over the data. Thus, Savitzky-Golay filter is a common name for polynomial filter.
**Text changes:** This was done through applying SG filters to the GLORIA temperature data in all three dimensions. For the SG filtering, 3rd order polynomials were fitted to 25, 60, and 60 neighbouring points in the vertical, zonal, and meridional directions.

**Reviewer comment:** Page 6, Figure 2, I feel Fig. 2 could be improved for better visulization. Add x - y - z coordinate to show the scale of wave structures. The colorbar for positive and negative temperature perturbation should be properly chosen (redwhite-blue) to clearly demonstrate the wave pattern. Figure 3 of Wright et al. 2017 is a good example.
**Authors response:** Fig. 2 will be changed according to the remarks.

**Reviewer comment:** Page 6, Line 1, direction-directions, taken-treated. Page 6, Line 2, can be seen - is demonstrated.
**Authors response:** This will be changed.

**Reviewer comment:** Page 7, Figure 3, the x-coordinate of bottom sub-figures could be just the distance, which is more straightforward to compare the scales of GWs.
**Authors response:** Fig. 3 D-F now plots distance as x-axis. Furthermore, the colormap of Fig. 3 will be changed to be in agreement with the updated Fig. 2.

**Reviewer comment:** Page 7, Line 8, and the data plotted in Fig. 2 and Fig. 3, what is the horizontal resolution of the raw temperature measurements? You may clarify these basic information in the text.
**Authors response:** This information can be found at the end of Sec. 2.1.

**Reviewer comment:** Page 7, Line 9, 3D direction- please clarify this direction, is this direction the wave propagation direction or the orientation of the wave front? You assume it is a mountain wave, so the wave is not really propagating. So if it is the orientation of the wave front, is there a relationship between the wave front orientation and the mountain ridge orientation?
**Authors response:** The 3D direction is the direction of the wave vector $\vec{k} = (k, l, m)$. And the wave vector is oriented perpendicular to the mountain ridge. 2 panels with the horizontal wave vector direction and the orography of Iceland will be added to Fig. 5 (*former Fig. 4*).
**Text changes:** The fitted parameters are the 3D wave vector $\vec{k} = (k, l, m)$ and the amplitudes (Fig. 5C). Horizontal and vertical wavelengths, and the horizontal wave direction were calculated from the wave vector $\vec{k}$ and shown in Fig. 5A, 5B, and 5E, respectively. Fig. 5F shows the orography of Iceland. The main mountain ridge is oriented in east-west direction. As expected for a mountain wave, the horizontal wave direction (Fig. 5E) is perpendicular to the ridge orientation.

**Reviewer comment:** Page 7, Line 14, the strength of the coupling of a GW with the background, what does this mean? Does it mean the same as the forcing/drag of GW. Page 7, Line 15, at the end add when they dissipate.
**Authors response:** The misleading expression 'strength of the coupling' will be replaced and the sentence will be reworded.
**Text changes:** Integrating the GWMF over the horizontal extent of a GW event leads to the total momentum, which determines the maximal drag this GW event can exert on the background flow in coupling and dissipation processes.

**Reviewer comment:** Page 8, Line 1, since those wave parameters are derived from fitting, are there confidence intervals that can describe the robustness of the fitting, say the uncertainties of those fitted parameters.
**Authors response:** A discussion of relevant effects for the uncertainty of the fitted parameters and the resulting confidence intervals is given in Appendix A. This will be mentioned here.

**Reviewer comment:** Page 8, Line 5-6, the total momentum in the order of GN (109N) seems to be a gigantic number, what is the physical meaning of this total momentum? The force the wave exerts on atmosphere? And how do you distinguish these two waves spatially?
**Authors response:** The total momentum corresponds to the maximal drag a GW event can exert on the background flow in coupling and dissipation processes. The two waves were defined to be north and south of 66.2° N. These points will be clarified in the text.
**Text changes:** The horizontal distribution of the GWMF clearly highlights two distinct wave packets: one with local GWMF of up to 50 mPa north of 66.2 ° N and one with local GWMF of up to 100 mPa south of 66.2 ° N. The GLORIA observations provide the horizontal variations of GWMF at 11.5 km altitude. This allows to integrate over the corresponding area of the two events and calculate the total momentum, a measure for the maximal drag this GW event can exert on the background flow in coupling and dissipation processes. This is a main advantage with respect to 1D wind observations, which can provide peak GWMF values but not the area for which these values are valid.

**Reviewer comment:** Page 8, Line 7, how do you quantify the GW and calculate MF from ECWMF model? Page 8, Line 8, how do you calculate this 0.14%? Do you mean the largest 0.14% of the all GWs?
**Authors response:** Similar points were mentioned by all three reviewers. We will include the details on how the occurrence probabilities are determined in the manuscript.
**Text changes:** To classify this event, a comparison of all GW events in January 2016 has been performed in the 6-hourly operational analyses of ECMWF. First the temperature background was isolated, as described in Sec. 2.1 for the a-priori field, and subtracted from the original field. The remaining temperature residuals were analyzed for GWs using the 3D sinusoidal fit algorithm described above. The GWMFs for all cubes were calculated. The GWMFs from all 124 analyses fields were combined to obtain the probability of GW occurrence (Fig. 6*, former Fig. 5*). Here, all GWMF values were considered independent of the horizontal and vertical wavelengths. Removing wavelengths larger than 2.5 times the cube size in order to filter less significant fits (not shown) induced no major changes in the general shape of the distribution. This indicates that GW events with less certain fits do not bias the probability distribution.
For the GW event over Iceland similar GWMF magnitudes were determined from the ECMWF analyses and from the GLORIA measurements. Thus, a comparison of the measurement results with the occurrence probability determined from the ECMWF analyses seems reasonable. According to Fig. 6 the measured GW event can be classified as a very strong case since the sum of all occurrence probabilities of stronger events is far below 1%.

**Reviewer comment:** Page 8, Line 14, characterize-locate or identify. Page 8, Line 15, advance-advantage.
**Authors response:** These points will be changed in the manuscript.

**Reviewer comment:** Page 8, Line 17, in this condition, when ray-tracing is discussed, GW intrinsic parameters rather than MF matter here.
**Authors response:** This will be changed in the text.

**Reviewer comment:** Page 9, Figure 5, this is the intermittency of the gravity waves, which is mainly described by this probability distribution. I suppose you can make a similar plot using the MF derived from your observations, which I think makes more sense to quantify the intermittency of the gravity waves retrieved from your observations. If go further, the log-normal distribution can also be fitted in the probability distributions.
**Authors response:** A similar distribution derived from GLORIA measurements cannot be provided, as tomographic measurement patterns are event based only and, thus, not suitable for a statistical analysis.

**Reviewer comment:** Page 9, Line 9-10, for each dot of different size, it could be better visualization if you add a white edge for each dot, then they can be still visible when overlapped with dense trajectories.
**Authors response:** Fig. 7 will be updated in this respect.

**Reviewer comment:** Page 9, Line 10-11, according to the GWMF at the source location, so here you implicitly assume the GWs do not undergo any dissipation when they propagate from source to measurement locations?
**Authors response:** This will be addressed in the revised manuscript.
**Text changes:** These GWMF values are conservative estimates, as the backward ray-tracing cannot account for dissipation processes.

**Reviewer comment:** Page 9, Line 13-14, what is the point of this 6 hour, in your Figure 6A, you indicate it is a 1-day backward simulation. So is there any conflict between these two? Then, can we understand this time is related to the propagating speed of the wave packet, say how much time it takes to propagate from source to measurement location. If so, a speed (group speed?) could be estimated.

**Authors response:** We constructed a GROGRAT background atmosphere allowing for backward integration up to one day. However, the rays actually arrived at the mountains already after 6 hours. This will be clarified in the text.
**Text changes:** As can be seen in Fig. 7C, the ray-traces need between 3 and 6 hours to reach the ground. This is in good agreement with a vertical group velocity of 2 to 3 km/h, which has been calculated from the measurements. Hence, the GWs are probably excited roughly 6 hours before the measurements were taken.

**Reviewer comment:** Page 10, Line 1-2, the turning of the wave vectors could be explained by the wave refraction.
**Authors response:** This explanation will be added to the manuscript.
**Text changes:** Over Eastern Europe, the GWs are refracted by a horizontal wind shear, which changes their horizontal wave vector from southward to westward. This allows the waves to quickly propagate upward into the westerly wind in the mid stratosphere.

**Reviewer comment:** Page 11, the ray-tracing simulation (backward and forward) of GW propagation and the comparsion between 1D vs. 4D run are dramatically interesting and important. I expect more discussions about the ray-tracing results, especially on how this study can advance our understanding of the horizontal propagation of GWs and insights into GW parameterization.
**Authors response:** The authors very much appreciate this comment and will extend the discussion, respectively.
**Text changes:** Two processes might play a significant role here: First, in the 1D GROGRAT version the GWs are not refracted and the wave vectors do not change its horizontal orientation with altitude. The westerly background winds at higher altitudes do not favor the propagation of GWs with wave vectors perpendicular to the wind direction. Second, in the full GROGRAT run, the GWs propagate horizontally away from the source. Hence, the GWs avoid the critical level positioned above the source location and more GWMF is transported to higher altitudes. Global mountain wave modeling (Xu et al., 2017) suggests that this effect may prevail also on a global basis.
Neither a realistic orientation of the wave vector, nor oblique GW propagation are incorporated in GW parameterizations used in current climate and weather prediction models (McLandress, 1998; Alexander and Dunkerton, 1999; Richter et al., 2010; McLandress et al., 2012; Garcia et al., 2017). However, both processes are context of several studies aiming to improve GW parameterizations (Preusse et al., 2009; Sato et al., 2009; Kalisch et al., 2014; Amemiya and Sato, 2016; Ribstein and Achatz, 2016; Garcia et al., 2017). The present paper provides a strong motivation to finally implement these processes in current climate and weather prediction models. Especially, as this could close gaps of GWMF in regions with sparse sources (McLandress et al., 2012) and reduce the cold-pole bias of climate and weather prediction models in the lower stratosphere (Garcia et al., 2017).

**Reviewer comment:** Page 14, Line 16, 60°.
**Authors response:** This will be changed in the text.

**Reviewer comment:** Page 17, please skip the questions regarding the uncertainties of fitted GW parameters.
**Authors response:** The authors think that the uncertainty discussion is an important part of this paper and therefore prefer to keep these paragraphs.

## Reviewer #3

**Reviewer comment:** Could you be more specific here regarding the regularization term or provide a reference where the use of this term is better detailed?
**Authors response:** More details on the used regularization can be found in **?**. This citation will be mentioned in the text.

**Reviewer comment:** Similarly, could you be more specific on the smoothing you are using in the raw ECMWF fields?
**Authors response:** More details will be included in the text.
**Text changes:** This smoothing was done by applying a low-pass Fourier filter with cut-off wavenumber 18 in zonal direction. In height and latitude direction Savitzky-Golay (SG) filter (Savitzky and Golay, 1964) was applied with 4th order polynomials over 11 and 25 neighbouring points respectively. On the one hand, the so generated a-priori field improves the convergence speed of the iterative minimization, as this temperature structure is close to the true values due to the high quality of the ECMWF model. On the other hand, the smoothening ensures that any GW signature in the retrieval result does not stem from the used a priori data. If the a-priori data exerts any influence, it would dampen the GW structure.

**Reviewer comment:** Could you please state the airplane altitude during GLORIA measurements?
**Authors response:** This point will be included in the manuscript.
**Text changes:** The aircraft flight altitude during this time was between 12.5 km and 13.5 km. Towards low altitudes, the GLORIA measurements were limited by clouds reaching up as far as 9 to 10.5 km.

**Reviewer comment:** One primary goal of the article is to show how GLORIA observations can be used to accurately retrieve gravity-wave fluctuations. I am therefore surprised that you did not try to show comparisons between

the retrieved 3D temperature field and in-situ observations performed by the airplane before the hexagonal path or with the dropsonde measurements, as well as with the resolved gravity-wave structures in the ECMWF analyses. In my opinion, such comparison should further support the capabilities of GLORIA, and perhaps also provide an additional way of characterizing the instrument performances.
**Authors response:** A comparison of the GLORIA measurements with in-situ measurements and ECMWF will be included as a new figure (Fig. 4). Both measurements agree well within the spatial resolution range of GLORIA.
**Text changes:** Fig. 4 shows a comparison of the retrieval results with in-situ measurements and ECMWF operational analyses with T1279/L137 resolution. The retrieval results and model data were interpolated onto the in-situ measurement locations. The GLORIA measurements agree well with the in-situ measurements. Some very short scales are beyond the spatial resolution of GLORIA. The ECMWF analysis catches the main variations, but the temperature oscillations are not as strong as in reality. GLORIA can better reproduce peaks as for example the one around 10:40 UTC. This comparison underlines the high quality of the GLORIA measurement data.

**Reviewer comment:** It may be worth stating that Equation (2) actually only applies in the socalled mid-frequency approximation, where pseudo-momentum and momentum fluxes are stricly equivalent. Otherwise, the sentence here may be slightly confusing. I furthermore wonder whether this approximation is really valid in this case study. The ratio of horizontal/vertical wavelengths seems to imply relatively long waves, for which inertial effects in Equation (2) could not be totally neglected.
**Authors response:** For the derivation of Equation (2), the mid-frequency approximation was not used. However, the low and high frequency terms of Equation (6) in **?** have been omitted as their impact on the result is below 1% in the measured gravity wave range. A full discussion of the importance of these low and high frequency terms can be found in **?**. This point will be clarified in the manuscript.
**Text changes:** Low and high frequency terms are omitted here due to simplicity. Deviations from the full equations derived by **?** are less than 1% in the observational range of GLORIA. For a full discussion of the relevance of all correction terms see the supporting information in **?**.

**Reviewer comment:** Section 3.1, last paragraph: this comparison looks somewhat biased to me: if I have well understood, the GWMF for the Iceland case study are in one hand estimated from GLORIA observations, while in the other hand they are compared to a distribution of GWMF computed with ECMWF operational analyses. There is actually no garanty that ECMWF analyses accurately resolve such mountain wave events, and e.g. **?** have reported a significant underestimation of GWMF in ECMWF operational analyses.
**Authors response:** This point was mentioned by all three reviewers. We will include the details on how the occurrence probabilities are determined in the manuscript. A comparison of GLORIA measurements with ECMWF shows that for the case discussed in our paper, the GWMFs have a similar magnitude. Therefore, we have confidence that the statistics derived from ECMWF are a meaningful way to set our event into a broader context.
**Text changes:** To classify this event, a comparison of all GW events in January 2016 has been performed in the 6-hourly operational analyses of ECMWF. First the temperature background was isolated, as described in Sec. 2.1 for the a-priori field, and subtracted from the original field. The remaining temperature residuals were analyzed for GWs using the 3D sinusoidal fit algorithm described above. The GWMFs for all cubes were calculated. The GWMFs from all 124 analyses fields were combined to obtain the probability of GW occurrence (Fig. 6*, former Fig. 5*). Here, all GWMF values were considered independent of the horizontal and vertical wavelengths. Removing wavelengths larger than 2.5 times the cube size in order to filter less significant fits (not shown) induced no major changes in the general shape of the distribution. This indicates that GW events with less certain fits do not bias the probability distribution.
For the GW event over Iceland similar GWMF magnitudes were determined from the ECMWF analyses and from the GLORIA measurements. Thus, a comparison of the measurement results with the occurrence probability determined from the ECMWF analyses seems reasonable. According to Fig. 6 the measured GW event can be classified as a very strong case since the sum of all occurrence probabilities of stronger events is far below 1%.

# References


Alexander, M. J. and Dunkerton, T. J.: A Spectral Parameterization of Mean-Flow Forcing due to Breaking Gravity Waves, Journal of the Atmospheric Sciences, 56, 4167–4182, doi:10.1175/1520-0469(1999)056¡4167:ASPOMF¿2.0.CO;2, 1999.

Amemiya, A. and Sato, K.: A New Gravity Wave Parameterization Including Three-Dimensional Propagation, Journal of the Meteorological Society of Japan. Ser. II, advpub, doi:10.2151/jmsj.2016-013, 2016.

Bossert, K., Fritts, D. C., Pautet, P.-D., Williams, B. P., Taylor, M. J., Kaifler, B., Drnbrack, A., Reid, I. M., Murphy, D. J., Spargo, A. J., and MacKinnon, A. D.: Momentum flux estimates accompanying multiscale gravity waves over Mount Cook, New Zealand, on 13 July 2014 during the DEEPWAVE campaign, J. Geophys. Res. Atmos., 120, 9323–9337, doi:10.1002/2015JD023197, URL http://dx.doi.org/10.1002/2015JD023197, 2015JD023197, 2015.

Cao, B., Heale, C. J., Guo, Y., Liu, A. Z., and Snively, J. B.: Observation and modeling of gravity wave propagation through reflection and critical layers above Andes Lidar Observatory at Cerro Pachn, Chile, J. Geophys. Res. Atmos., 121, 12,737–12,750, doi:10.1002/2016JD025173, URL http://dx.doi.org/10.1002/2016JD025173, 2016JD025173, 2016.

Garcia, R. R., Smith, A. K., Kinnison, D. E., de la Camara, A., and Murphy, D. J.: Modification of the Gravity Wave Parameterization in the Whole Atmosphere Community Climate Model: Motivation and Results, J. Atmos. Sci., 74, 275–291, doi:10.1175/JAS-D-16-0104.1, 2017.

Kalisch, S., Preusse, P., Ern, M., Eckermann, S. D., and Riese, M.: Differences in gravity wave drag between realistic oblique and assumed vertical propagation, Journal of Geophysical Research: Atmospheres, 119, 10,081–10,099, doi:10.1002/2014JD021779, 2014.

Lu, X., Chen, C., Huang, W., Smith, J. A., Chu, X., Yuan, T., Pautet, P.-D., Taylor, M. J., Jie, G., and Cullens, C. Y.: A coordinated study of 1 h mesoscale gravity waves propagating from Logan to Boulder with CRRL Na Doppler lidars and temperature mapper, J. Geophys. Res. Atmos., 120, 10,006–10,021, doi:10.1002/2015JD023604, URL http://dx.doi.org/10.1002/2015JD023604, 2015JD023604, 2015.

McLandress, C.: On the importance of gravity waves in the middle atmosphere and their parameterization in general circulation models, J. Atm. Sol.-Terr. Phys., 60, 1357–1383, doi:10.1016/S1364-6826(98)00061-3, 1998.

McLandress, C., Shepherd, T. G., Polavarapu, S., and Beagley, S. R.: Is Missing Orographic Gravity Wave Drag near 60S the Cause of the Stratospheric Zonal Wind Biases in Chemistry-Climate Models?, J. Atmos. Sci., 69, 802–818, doi:10.1175/JAS-D-11-0159.1, URL http://dx.doi.org/10.1175/JAS-D-11-0159.1, 2012.

Preusse, P., Eckermann, S. D., Ern, M., Oberheide, J., Picard, R. H., Roble, R. G., Riese, M., Russell III, J. M., and Mlynczak, M. G.: Global ray tracing simulations of the SABER gravity wave climatology, J. Geophys. Res. Atmos., 114, doi:10.1029/2008JD011214, 2009.

Ribstein, B. and Achatz, U.: The interaction between gravity waves and solar tides in a linear tidal model with a 4-D ray-tracing gravity-wave parameterization, Journal of Geophysical Research: Space Physics, 121, 8936–8950, doi:10.1002/2016JA022478, URL http://dx.doi.org/10.1002/2016JA022478, 2016JA022478, 2016.

Richter, J. H., Sassi, F., and Garcia, R. R.: Toward a Physically Based Gravity Wave Source Parameterization in a General Circulation Model, Journal of the Atmospheric Sciences, 67, 136–156, doi:10.1175/2009JAS3112.1, 2010.

Sato, K., Watanabe, S., Kawatani, Y., Tomikawa, Y., Miyazaki, K., and Takahashi, M.: On the origins of mesospheric gravity waves, Geophys. Res. Lett., 36, doi:10.1029/2009GL039908, 2009.

Savitzky, A. and Golay, M. J. E.: Smoothing and Differentiation of Data by Simplified Least Squares Procedures., Analytical Chemistry, 36, 1627–1639, doi:10.1021/ac60214a047, URL http://dx.doi.org/10.1021/ac60214a047, 1964.

Stober, G., Sommer, S., Rapp, M., and Latteck, R.: Investigation of gravity waves using horizontally resolved radial velocity measurements, Atmos. Meas. Tech., 6, 2893–2905, doi:10.5194/amt-6-2893-2013, URL http://www.atmos-meas-tech.net/6/2893/2013/, 2013.

Xu, X., Wang, Y., Xue, M., and Zhu, K.: Impacts of Horizontal Propagation of Orographic Gravity Waves on the Wave Drag in the Stratosphere and Lower Mesosphere, J. Geophys. Res. Atmos., doi:10.1002/2017JD027528, URL http://dx.doi.org/10.1002/2017JD027528, 2017JD027528, 2017.

# First tomographic observations of gravity waves by the infrared limb imager GLORIA

Isabell Krisch[1], Peter Preusse[1], Jörn Ungermann[1], Andreas Dörnbrack[2], Stephen D. Eckermann[3], Manfred Ern[1], Felix Friedl-Vallon[4], Martin Kaufmann[1], Hermann Oelhaf[4], Markus Rapp[2,5], Cornelia Strube[1], and Martin Riese[1,6]

[1]Forschungszentrum Jülich, Institute of Energy- and Climate Research, Stratosphere (IEK-7), Jülich, Germany
[2]Deutsches Zentrum für Luft- und Raumfahrt, Institut für Physik der Atmosphäre, Oberpfaffenhofen, Germany
[3]E. O. Hulburt Center for Space Research, Naval Research Laboratory, Washington, D.C., USA.
[4]Karlsruhe Institute of Technology, Institute of Meteorology and Climate Research, Karlsruhe, Germany
[5]Meteorologisches Institut München, Ludwig-Maximilians-Universität München, Munich, Germany
[6]Institut für Atmosphären- und Umweltforschung, Bergische Universität Wuppertal, Wuppertal, Germany

*Correspondence to:* I. Krisch (i.krisch@fz-juelich.de)

**Abstract.** Atmospheric gravity waves are a major cause of uncertainty in atmosphere general circulation~~global atmospheric~~ (RC2: #1,#6) models. This uncertainty affects regional climate projections and seasonal weather predictions. Improving the representation of gravity waves in general circulation~~global atmospheric~~ (RC2: #1,#6) models, is therefore of primary interest. In this regard, measurements providing an accurate 3D characterization of gravity waves are needed. Using the Gimballed Limb Observer for Radiance Imaging of the Atmosphere (GLORIA), the first airborne implementation of a novel infrared limb imaging technique, a gravity wave event over Iceland was observed~~measured~~ (RC2: #2). An air volume disturbed by this gravity wave, was investigated from different angles by encircling the volume with a closed flight pattern. Using a tomographic retrieval approach, the measurements of this air mass under different angles allowed for a 3D reconstruction of the temperature and trace gas structure. The temperature measurements were used to derive gravity wave amplitudes, 3D wave vectors, and direction-resolved momentum fluxes. These parameters facilitated the backtracing of the waves to their sources on the south coast of Iceland. Two wave packets are distinguished, one stemming from the main mountain ridge in the South of Iceland, a second one from the smaller mountains in the North. The total, area-integrated fluxes of these two wave packets are determined. Forward ray-tracing reveals that the waves propagate laterally more than 2000 km away from their source region. A comparison of a 3D ray-tracing version to solely column based propagation showed that lateral propagation can help the waves to avoid critical layers and propagate to higher altitudes. Thus, the implementation of oblique gravity wave propagation into general circulation models may improve their predictive skills.~~Following the waves forward with a ray-tracing model highlighted the importance of 3D propagation, an effect generally neglected in global atmospheric models.~~ (RC2: #3)

## 1 Introduction

Gravity waves (GWs) are oscillations in wind velocity and temperature with buoyancy as restoring force (Fritts and Alexander, 2003). They are the main driver of prominent circulation patterns in the mesosphere, such as the wind reversal in the meso-

sphere – lower thermosphere region (MLT). The exerted drag induces the meridional circulation in the MLT and finally leads to~~Thereby, they are responsible for~~ (RC2: #4) the cold summer mesopause and the warm winter stratopause (Holton, 1982, 1983; McLandress, 1998; Siskind, 2014).

GWs not only have a strong influence on the mesosphere but also on the stratosphere. There, they influence the circumpolar jet and its varying degrees of strength (McLandress et al., 2012; Ern et al., 2016); the tropical quasi-biennial-oscillation (QBO) (RC2: #5) of stratospheric tropical winds and its teleconnections into the extratropical troposphere (Dunkerton, 1997; Kawatani et al., 2010; Ern et al., 2014); and the variability in the strength of the meridional Brewer Dobson circulation (Alexander and Rosenlof, 2003; Butchart, 2014). These stratospheric circulations then have an impact on near-surface seasonal weather and regional climate via dynamical couplings with the troposphere (Scaife et al., 2016; Kidston et al., 2015).

Considering their small scales, the full spectrum of GWs cannot be resolved in general circulation models (GCMs) due to computational issues.~~Considering their small scales, GWs cannot be resolved in global atmospheric circulation models (GCMs) due to computational issues.~~ (RC2: #6) Hence, they are simplified in form of parameterizations. Consequences of these GW parameterizations are for example surface temperature uncertainties of up to 2 K (Sigmond and Scinocca, 2010) and pressure discrepancies of several hPa at polar latitudes (Sandu et al., 2016) in climate projections. Improved weather predictions and climate projections therefore require more advanced parameterization schemes as proposed by various studies (Kim et al., 2013; Bushell et al., 2015; de la Camara and Lott, 2015; Amemiya and Sato, 2016).

One of the strongest simplifications, used for parameterizations, is to assume solely vertical propagation of GWs. However, several modelling studies, have highlighted the importance of 3D propagation of GWs to correctly reproduce the above mentioned circulation patterns (Sato et al., 2009; Preusse et al., 2009; McLandress et al., 2012; Kalisch et al., 2014; Ribstein and Achatz, 2016). Further, GW source distributions and launch parameters, such as propagation direction and wavelength spectrum, (RC2: #8) are often over-simplified in parameterizations (McFarlane, 1987; Hines, 1997; Alexander and Dunkerton, 1999; Scinocca and McFarlane, 2000; Beres et al., 2005; Richter et al., 2010; Garcia et al., 2017) (RC2: #7) and need validation by observations (Geller et al., 2013).

To underline the importance of 3D propagation and validate GW source distributions, measurements are needed, which allow for a full 3D wave characterization including the propagation direction (Alexander et al., 2010). Such a characterization is, in principle, possible from various in-situ techniques. Several methods were developed to evaluate data from close-to-vertical profiles taken by radiosondes, dropsondes or falling spheres. These methods include hodograph analysis (Guest et al., 2000), Stokes method (Eckermann and Vincent, 1989) or a combination of wind and temperature measurements in a common approach (Wang and Geller, 2003; Zhang et al., 2014). Furthermore, there are multiple techniques based on horizontal traces for example from airplane measurements (Alexander and Pfister, 1995; Fritts et al., 2016; Smith et al., 2016; Wagner et al., 2017) and observations by superpressure balloons (Boccara et al., 2008; Hertzog et al., 2008). All these methods have in common that they infer the wave direction via polarization~~polarisation~~ (RC2: #9) and dispersion relations and do not reveal the 3D wave structure directly.

First 3D wave structures from satellite measurements in the stratosphere are presented by Ern et al. (2017) and Wright et al. (2017). However, these studies are based on nadir observations of the Atmospheric Infrared Sounder (AIRS) satellite

instrument and are limited by the coarse vertical resolution. This implies that GWs with vertical wavelengths below 15 km are invisible to the instrument. In the mesosphere, a full wave characterization of short scale GWs has been achieved with the Middle Atmosphere Alomar Radar System (MAARSY; Stober et al., 2013). For medium scale GWs in the mesosphere, a full characterization has been derived by combining lidar and airglow imager measurements (Bossert et al., 2015; Lu et al., 2015; Cao et al., 2016). However, all these ~~Such~~ (RC2: #10) observations are limited to a few ground based stations. Further, it is difficult to link observations at altitudes as high as the mesopause region to specific GW sources, which are usually located at much lower altitudes in the troposphere and lower stratosphere. So far no measurement technique existed to measure the 3D structure of mesoscale GWs in the lower stratosphere.

A novel technique to measure GWs in the upper troposphere – lower stratosphere, i.e. close to the GW sources, is limb imaging. Limb imaging allows for a 3D reconstruction of the atmospheric temperature and consequently a full characterization of mesoscale GWs. The development of the Gimballed Limb Observer for Radiance Imaging of the Atmosphere (GLORIA) is the first implementation of such an airborne infrared limb imager (Friedl-Vallon et al., 2014; Riese et al., 2014).

This technique was applied for the exploration of a GW for the first time in a research flight on 25 January 2016 above Iceland. The results of this research flight are presented in this paper. Section 2.1 describes the instrument and the retrieval technique. The ~~measurement~~ (RC2: #11) results are presented in section 2.2 and subsequently analyzed~~analysed~~ (RC2: #9) for GWs in section 3.1. The obtained GW parameters are used for a wave propagation study in section 3.2.

## 2 Data and methodology~~Measurements~~ (RC2: #12)

### 2.1 Measurement technique

This paper is based on tomographic measurements taken by the infrared limb imager GLORIA on board the German high altitude – long range research aircraft (HALO). The aircraft campaign took place from December 2015 to March 2016 with campaign bases in Kiruna, Sweden, and Oberpfaffenhofen, Germany. In total there were 21 research flights performed covering 20°N to 90°N and 80°W to 30°E. The scientific targets of this campaign were to demonstrate the use of infrared limb imaging for gravity wave studies (GWEX), to study the full life cycle of a gravity wave (GW-LCYCLE), to investigate the Seasonality of Air mass transport and origin in the Lowermost Stratosphere (SALSA), and to observe the Polar Stratosphere in a Changing Climate (POLSTRACC).

GLORIA combines a Michelson interferometer with a two-dimensional infrared detector and measures molecular thermal emissions in the spectral range between 780 $\mathrm{cm}^{-1}$ and 1400 $\mathrm{cm}^{-1}$ (7.1 to 12.8 µm). It has a 256x256 pixels detector. However, to increase the read-out time, only a subset of 48x128 pixels is used. Thus, 6144 spectra are recorded simultaneously ~~recording 6144 spectra simultaneously~~ (RC2: #13). GLORIA's line-of-sight aims towards the horizon on the right side of the aircraft and measures infrared radiation emitted by molecules in the atmosphere. The point of the line-of-sight which is closest to the earth surface is called tangent point. Due to the curvature of the earth surface and the atmospheric density profile, the weighting function of the measurement signal has its maximum around this tangent point (Riese et al., 1999). This means that typically most of the measured radiation is emitted around the tangent points, which are located between 5 km and aircraft flight altitude.

The horizontal observation angle of GLORIA can be adjusted from 45° (right-forward) to 135° (right-backward) in respect to the aircraft's flight direction. In this way, the instrument can investigate the same air volume from different directions, which allows for a tomographic retrieval scheme (Ungermann et al., 2010; Kaufmann et al., 2015).

The basis of a tomographic retrieval scheme is a fast radiative transfer model. For the retrievals presented in this paper the Juelich Rapid Spectral Simulation Code Version 2 (JURASSIC2; Ungermann et al., 2010) is used. With this radiative transfer model $\boldsymbol{F}(\boldsymbol{x})$ infrared radiances can be calculated directly from an atmospheric state $\boldsymbol{x} \in \mathbb{R}^n$. Reconstructing the atmospheric state $\boldsymbol{x}$ from the infrared measurements $\boldsymbol{y} \in \mathbb{R}^m$ (the so called retrieval or inverse modelling) in contrast presents a non-linear inverse problem, which is solved with an iterative minimization approach (Ungermann et al., 2011, 2015). For this, the cost-function

$$J(\boldsymbol{x}) = (\boldsymbol{F}(\boldsymbol{x}) - \boldsymbol{y})^T \mathbf{S}_\epsilon^{-1} (\boldsymbol{F}(\boldsymbol{x}) - \boldsymbol{y}) \tag{1}$$

has to be minimized. Here $\mathbf{S}_\epsilon \in \mathbb{R}^{m \times m}$ represents the covariance matrix of the measurement error $\epsilon$. To get a unique and well-constrained solution to this minimization problem, a regularization term is added to the cost-function (Ungermann et al., 2010) (RC3: #1). This term ensures that the solution is physically reasonable.

As a-priori field $\boldsymbol{x}_a$ a temperature field from the European Centre for Medium-Range Weather Forecasts (ECMWF) operational analyses at resolution T1279/L137 was used, which was smoothed in all spatial directions to remove GW signatures. This smoothing was done by applying a low-pass Fourier filter with cut-off wavenumber 18 in zonal direction. In height and latitude direction a Savitzky-Golay (SG) filter (Savitzky and Golay, 1964) was applied with 4th order polynomials over 11 and 25 neighbouring points respectively. On the one hand, the so generated a-priori field improves the convergence speed of the iterative minimization, as this temperature structure is close to the true values due to the high quality of the ECMWF model.~~In this way, on the one hand, the convergence speed of the iterative minimization is improved, as the temperature background structure is close to the true values due to the high quality of the ECMWF model.~~ (RC1: #1 & RC3: #2) On the other hand, the smoothening ensures that any GW signature~~structure~~ (RC2: #16) in the retrieval result does not stem from the used a priori data. If the a-priori data exerts any influence, it would dampen the GW structure.

For the present retrieval we used the spectral ranges listed in Tab. 1. In these spectral ranges the main emitters are $CO_2$, $CCl_4$, $HNO_3$, and $O_3$. The volume mixing ratio of $CO_2$ is well known in this altitude range~~in this part of the atmosphere~~ (RC2: #17). Therefore, spectral lines of $CO_2$ are used effectively for the retrieval of temperature. Tomographic reconstructions of the 3D temperature distribution and the mixing ratios of $CCl_4$, $HNO_3$, and $O_3$ in the upper troposphere and lower stratosphere were achieved. However, a discussion of the trace gas distributions exceeds the scope of this paper.

An error analysis of the retrieval has been performed following the methods described in Ungermann et al. (2015). The precision (noise error) is below 0.05 K and the accuracy, which includes misrepresented background gases, uncertainties in spectral line characterisation, uncertainties in instrument attitude, and calibration errors, is in the order of 0.5 K.

The horizontal and vertical resolutions can be defined by the axes of the smallest ellipsoid containing all elements of the averaging kernel larger than half the maximum. Accordingly, in the middle of the performed hexagonal flight path, the vertical resolution is around 200 m, the horizontal resolution around 20 km.~~The vertical resolution can be defined as the full width at~~

**Table 1.** Spectral windows used for the retrieval presented in this paper. The last column indicates the retrieved quantity for each spectral range~~which window is used for which retrieval quantity~~ (RC2: #15).

| | spectral range / $cm^{-1}$ | | | used for |
|---|---|---|---|---|
| 1 | 790.625 | – | 792.500 | temperature |
| 2 | 793.125 | – | 795.000 | $CCl_4$ |
| 3 | 796.875 | – | 799.375 | $CCl_4$ |
| 4 | 883.750 | – | 888.125 | $HNO_3$ |
| 5 | 892.500 | – | 896.250 | $HNO_3$ |
| 6 | 900.000 | – | 903.125 | $HNO_3$ |
| 7 | 918.750 | – | 923.125 | $HNO_3$ |
| 8 | 956.875 | – | 962.500 | temperature |
| 9 | 980.000 | – | 984.375 | temperature, $O_3$ |
| 10 | 992.500 | – | 997.500 | temperature, $O_3$ |
| 11 | 1000.625 | – | 1006.250 | temperature, $O_3$ |
| 12 | 1010.000 | – | 1014.375 | temperature, $O_3$ |

~~half maximum of averaging kernel matrix and is around 200 m at an altitude of 11.5 km. The diameter of the smallest sphere containing all elements of the averaging kernel larger than half the maximum, which is a measure for the horizontal resolution , is around 20 km inside the performed hexagonal flight path.~~ (RC1: #2)

The time needed to accomplish the hexagon was about 2 h. During this time 2200 infrared images and corresponding spectra were taken. The presented tomographic retrieval represents a temporal mean over all these measurements. (RC2: #18)

### 2.2 Research flight above Iceland

On the measurement day 25 January 2016, a southerly wind made landfall on the south coast of Iceland (Fig. 1), thus exciting mountain waves. These waves were predicted by the ECMWF forecast to be stationary above Iceland for more than 6 hours. (RC2: #19) Above 10 km altitude the zonal wind increased drastically with height and turned from southerly to southwesterly direction. This created a strong vertical wind shear, which influenced the propagation of the excited mountain waves ~~as discussed in Sec. 3.2~~ (RC2: #20). The wave structure over eastern Iceland was encircled by a hexagonal flight pattern with 460 km diameter between 10 and 12 UTC (Fig. 2). The aircraft flight altitude during this time was between 12.5 km and 13.5 km. Towards low altitudes, the GLORIA measurements were limited by clouds reaching up as far as 9 to 10.5 km. (RC3: #3 & RC2: #14) Before the hexagon a linear flight through the wave field has been performed to collect in-situ data at flight altitude and to release dropsondes.

For the GLORIA retrieval only the measurements taken between 10 and 12 UTC have been taken into account. To identify GWs in the retrieved 3D temperature field, the large scale temperature background, which is caused by the balanced flow

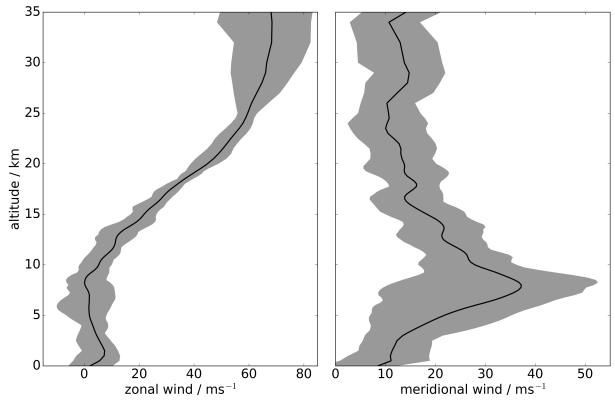


**Figure 1.** Mean zonal and meridional wind profiles from ECMWF operational analyses T1279/L137 above Iceland and the measurement region at 12 UTC on January 25, 2016. The grey area marks the spread of the wind profiles in this area.

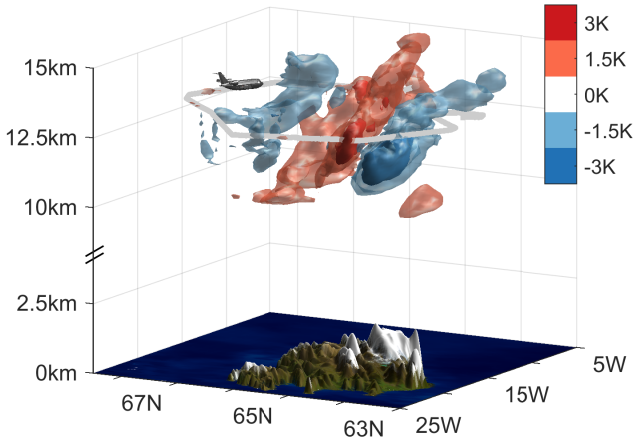


**Figure 2.** Tomographic retrieval of the temperature field for the research flight on January 25, 2016, over Iceland. Shown are isosurfaces of the temperature residual. The grey line around the retrieved 3D pattern indicates the flightpath.

and the stratification of the atmosphere, has to be separated from the smaller scale temperature variations caused by the GWs (RC2: #21). This was done through applying SG filters with 3rd order polynomials over 25, 60, and 60 neighbouring points in vertical, zonal, and meridional direction. ~~This was done through applying a Savitzky-Golay (SG) filter (Savitzky and Golay, 1964) to the GLORIA temperature data in all three dimensions. Therefore, 3rd order polynomials were fitted to 25, 60, and 60 neighbouring points in the vertical, zonal, and meridional direction.~~ (RC2: #22) The values of these polynomials at the respective points are treated~~taken~~ (RC2: #23) as temperature background. The remaining temperature residuals clearly reveal the complex structure of the wave field, which is demonstrated~~can be seen~~ (RC2: #24) in 3D in Fig. 2.

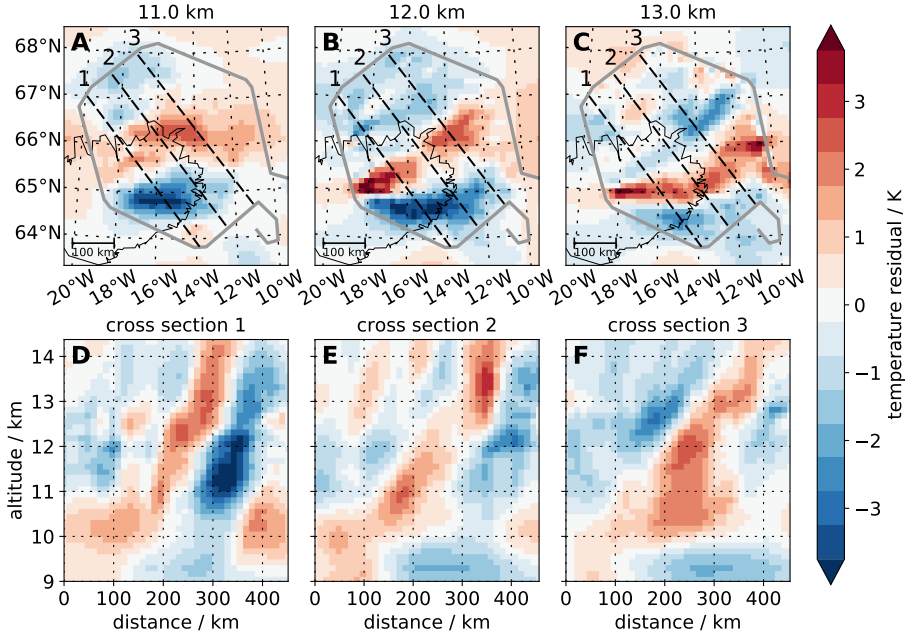


**Figure 3.** Horizontal (A-C) and vertical (D-F) cross sections through the 3D volume shown in Fig. 2. The grey line marks the flightpath. The locations of the vertical cross sections are indicated by numbered dashed lines.

In Fig. 3, horizontal and vertical cross sections through the measurement volume are presented. They show how the wave structure varies with height and horizontal location. For instance, the wave fronts directly above Iceland (64°N to 65.5°N and 14°W to 18°W are aligned east-west and tilted southwards against the prevailing southerly wind (Fig. 1). Further to the north-east (65°N to 67°N and 10°W to 14°W), the horizontal orientation of the wave fronts turns more into south-west to north-east. The horizontal wavelength varies inside the hexagon from 100 km up to 350 km. The vertical wavelength of the waves is between 3 km and 6 km. The temperature residuals range from ±4 K (in the south-west of the hexagon at an altitude of 12 km, 64°N to 65.5°N, and 14°W to 18°W) down to ±1 K (in the smaller scale waves in the north-western part of the hexagon at 66°N to 68°N and 16°W to 20°W).

Fig. 4 shows a comparison of the retrieval results with in-situ measurements and ECMWF operational analyses with T1279/L137 resolution. The retrieval results and model data were interpolated onto the in-situ measurement locations. The GLORIA measurements agree well with the in-situ measurements. Some very short scales are beyond the spatial resolution of GLORIA. The ECMWF analysis catches the main variations, but the temperature oscillations are not as strong as in reality. GLORIA can better reproduce peaks as for example the one around 10:40 UTC. This comparison underlines the high quality of the GLORIA measurement data. (RC3: #3)

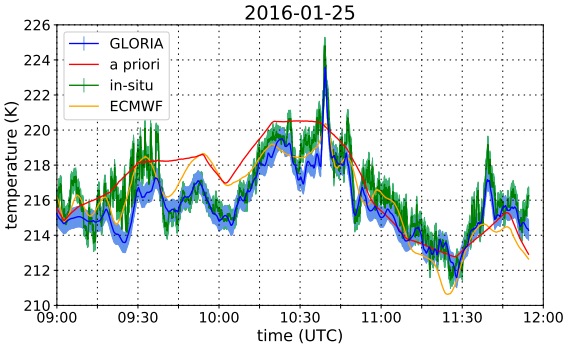


**Figure 4.** A comparison of the GLORIA retrieval results to in-situ temperature measurements and ECMWF operational analyses T1279/L137 at 12 UTC. The GLORIA retrieval and the ECMWF data were interpolated in space onto the flight path.

## 3 ResultsAnalysis (RC2: #27)

### 3.1 Sinusoidal wave fits

In order to further interpret the GW structure and fully characterize it, wave parameters are derived using a small-volume few-wave decomposition technique (Lehmann et al., 2012). The algorithm performs 3D sinusoidal fits in small data cubes. In such a way, the wave amplitude, horizontal and vertical wavelengths, and 3D wave direction can be derived. In contrast to a Fourier transform, this technique allows for the characterization of waves with wavelengths larger than the cube size (up to a factor of 2.5 times the cube size). Due to the prevailing wavelength range in our measurements (cf. Fig. 2), a cube size of 160 km x 160 km x 3.6 km, containing 4900 data points, was chosen. The fitted parameters are the 3D wave vector $\boldsymbol{k} = (k, l, m)$ and the amplitudes (Fig. 5C). Horizontal and vertical wavelengths, and the horizontal wave direction were calculated from the wave vector $\boldsymbol{k}$ and shown in Fig. 5A, 5B, and 5E, respectively. Fig. 5F shows the orography of Iceland. The main mountain ridge is oriented in east-west direction. As expected for a mountain wave, the horizontal wave direction (Fig. 5E) is perpendicular to the ridge orientation.~~the horizontal (Fig. 5A) and vertical (Fig. 5B) wavelengths, including the 3D direction of the wave vector and the amplitudes (Fig. 5C) of the waves.~~ (RC2: #29) A discussion of relevant effects for the uncertainty of the fitted parameters and the resulting confidence intervals is given in Appendix A. (RC2: #32)

A key quantity of GWs is the vector of vertical flux of horizontal pseudo-momentum (short GW momentum flux, GWMF)

$$\boldsymbol{F_{ph}} = \frac{1}{2}\rho\frac{\boldsymbol{k_h}}{m}\left(\frac{g}{N}\right)^2\left(\frac{\hat{T}}{T}\right)^2 \tag{2}$$

where $\rho$ represents the air density, $\boldsymbol{k_h} = (k, l)$ the horizontal and $m$ the vertical component of the wave vector~~$\boldsymbol{k_h}$ the horizontal and vertical wavenumbers~~ (RC2: #29), $g$ the standard gravity, $N$ the buoyancy, $T$ the background temperature, and $\hat{T}$ the temperature amplitude (Ern et al., 2004). Low and high frequency terms are omitted here due to simplicity. Deviations from

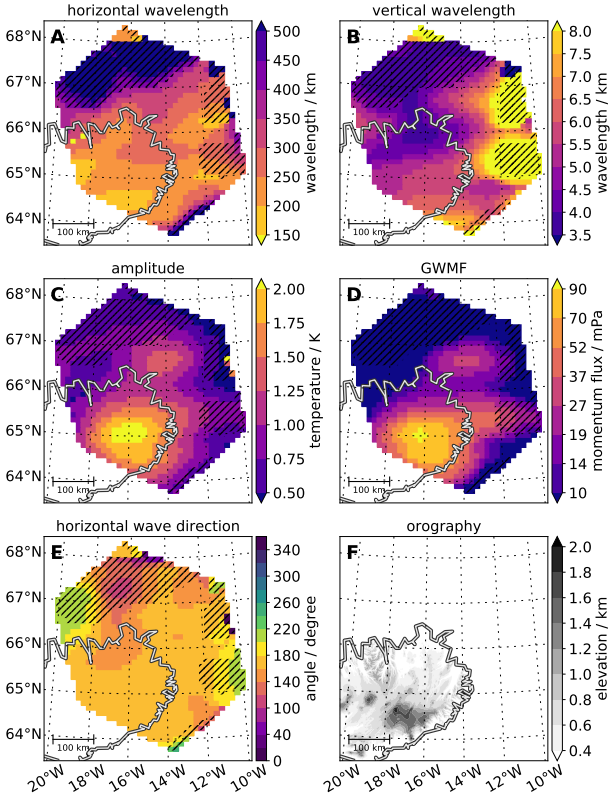


**Figure 5.** 3D sinusoidal wave fit of the GLORIA measurements in fitting cubes of 160 km x 160 km x 3.6 km at a center height of 11.5 km. Non-significant fitting results with wavelengths above 2.5 times the cube size are hashed. These parameters are used to drive the GROGRAT model, the results of which are shown in Fig. 7. Panel E shows the direction of the horizontal wave vector. Eastward direction corresponds to 90 °, southward direction to 180 °. (RC2: #29)

the full equations derived by Ern et al. (2004) are less than 1% in the observational range of GLORIA. For a full discussion of the relevance of all correction terms see the supporting information in Ern et al. (2017). (RC3: #4)

Integrating the GWMF over the horizontal extent of a GW event leads to the total momentum, which determines the maximal drag this GW event can exert on the background flow in coupling and dissipation processes. ~~The GWMF is a measure for the momentum carried by a GW and determines the strength of the coupling of a GW with the background and how much drag a GW can exert on the atmosphere.~~ (RC2: #30 & #31 & #33) The fitted wave parameters in Fig. 5A - C are used to calculate the GWMF (Fig. 5D). The horizontal distribution of the GWMF clearly highlights two distinct wave packets: one with local GWMF of up to 50 mPa north of 66.2 °N and one with local GWMF of up to 100 mPa south of 66.2 °N. The GLORIA observations provide the horizontal variations of GWMF at 11.5 km altitude. This allows to integrate over the corresponding area of the two events and calculate the total momentum, a measure for the maximal drag this GW event can exert on the background flow in coupling and dissipation processes. This is a main advantage with respect to 1D wind observations, which

can provide peak GWMF values but not the area for which these values are valid.~~around 66.5°N, 14°W and one with local GWMF of up to 100 mPa south of 66.2°N and between 14°W and 18°W. This distribution of GWMF allows for the estimation of the total momentum contained in these GW packets, if we integrate over their respective area.~~ (RC2: #33) The wave packet further south has a total momentum of 2.7 GN, the second wave packet further north only 0.4 GN. The total momentum of all the measured GWs above Iceland is 3.1 GN.

To classify this event, a comparison of all GW events in January 2016 has been performed in the 6-hourly operational analyses of ECMWF. First the temperature background was isolated, as described in Sec. 2.1 for the a-priori field, and subtracted from the original field. The remaining temperature residuals were analyzed for GWs using the 3D sinusoidal fit algorithm described above. The GWMFs for all cubes were calculated. The GWMFs from all 124 analyses fields were combined to obtain the probability of GW occurrence (Fig. 6). Here, all GWMF values were considered independent of the horizontal and vertical wavelengths. Removing wavelengths larger than 2.5 times the cube size in order to filter less significant fits (not shown) induced no major changes in the general shape of the distribution. This indicates that GW events with less certain fits do not bias the probability distribution. (RC1: #3, RC2: #34 & #35, RC3: #5)

For the GW event over Iceland similar GWMF magnitudes were determined from the ECMWF analyses and from the GLORIA measurements. Thus, a comparison of the measurement results with the occurrence probability determined from the ECMWF analyses seems reasonable. According to Fig. 6 the measured GW event can be classified as a very strong case since the sum of all occurrence probabilities of stronger events is well below 1%.~~(Fig. 6). This indicates our event as very strong as only 0.14% of all GW occurrences during this period have a higher GWMF.~~ (RC1: #3, RC2: #34 & #35, RC3: #5) This occurrence frequency is in good agreement with Alexander et al. (2010), Hertzog et al. (2012), and Podglajen et al. (2016) who present satellite and super-pressure balloon measurements at slightly higher altitudes.

### 3.2 Wave propagation with GROGRAT

In order to identify the GW source, we used the Gravity wave Regional Or Global RAy Tracer (GROGRAT; Marks and Eckermann, 1995). GROGRAT describes the propagation of wave packets based on linear wave theory. Backward ray-tracing has been used in previous studies to locate~~characterize~~ (RC2: #36) GW sources (Preusse et al., 2014; Pramitha et al., 2015). In order to initialize a ray-tracer, the wave must be fully characterized. This capability is the main improvement~~advance~~ (RC2: #37, advantage as proposed by reviewer changes the meaning of the sentence.) of the GLORIA observations compared (RC2: #37) to previous remote sensing observations of temperature. GW parameters obtained from single vertical temperature profiles, lead to a cone of potential source regions instead of a precise source location (Gerrard et al., 2004). This is the reason why GWs derived from conventional limb scanner measurements have~~GWMF data from conventional limb scanners has~~ (RC2: #38) not been interpreted in terms of backward ray-tracing. Only the 3D nature and accuracy of the GLORIA measurements allows backtracing to the precise source location. This is further highlighted by the error analysis presented in appendix A.

In the error analysis, a systematic low bias of the vertical wavelengths was found, which is caused by the sinusoidal fit (appendix A). Therefore, the vertical wavelengths from the sinusoidal fits were scaled by a factor 1.1, according to the determined

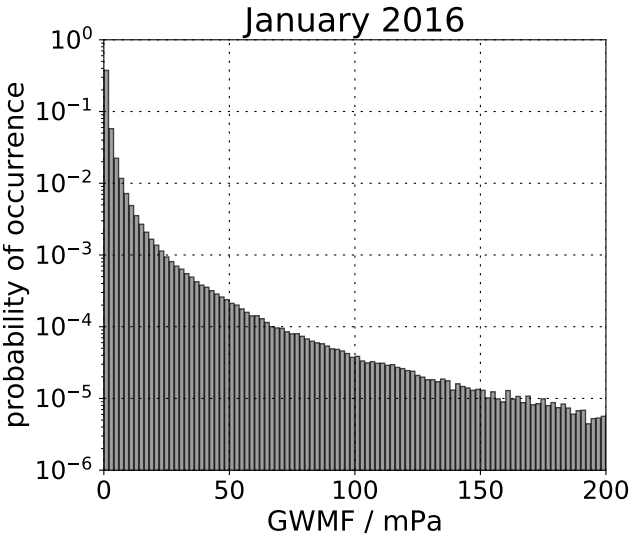


**Figure 6.** Probability of occurrence for GWs with specific momentum flux at 11.5 km altitude in a latitude band between 60°N and 70°N in January 2016 calculated from 6-hourly ECMWF operational analyses fields.

bias, before being used for the ray-tracing. For the propagation of GWs in a ray-tracing model temporally and spatially varying background temperature and wind fields are needed, which were obtained from ECMWF operational analyses.

Fig. 7 shows the backward ray-traces of the measured GWs from their measurement position (black crosses) down to the source location (red dots). The measurement position has been defined as the center point of the sinusoidal fitting cube. The strength of the GW is expressed by the size of the red dots, which has been chosen according to the GWMF at the source location. These GWMF values are conservative estimates, as the backward ray-tracing cannot account for dissipation processes. (RC2: #41) The source locations of the GWs, and in particular those of the highest GWMF, gather around the main mountain ridge of Iceland. The GWs are, thus, likely to have been excited by the southerly wind approaching these mountains. The ray-traces from the wave packet measured further in the north partly stop in the north of the island at single mountain peaks. ~~about 6 hours before the measurements. The ray-traces from the wave packet measured further in the north partly also stop in the north of the island at single mountain peaks.~~ (RC2: #42)

As can be seen in Fig. 7C, the ray-traces need between 3 and 6 hours to reach the ground. This is in good agreement with a vertical group velocity of 2 to 3 km/h, which has been calculated from the measurements. Hence, the GWs are probably excited roughly 6 hours before the measurements were taken. (RC2: #42)

Forward ray tracing is used to examine the propagation of the GWs away from the measurement location (Fig. 7B). On the measurement day, the southerly wind turned into a strong westerly direction above 10 km, creating a strong vertical wind shear. In this wind shear the GWs started to propagate eastward. This is confirmed by the measurements: at 11 km (Fig. 3A) the GWs are mainly located above the eastern part of Iceland, while at 13 km (Fig. 3C) the wave fronts already stretch far across the ocean. The waves require about one day to propagate to an altitude of 20 km (Fig. 7C). At the same time, they travel

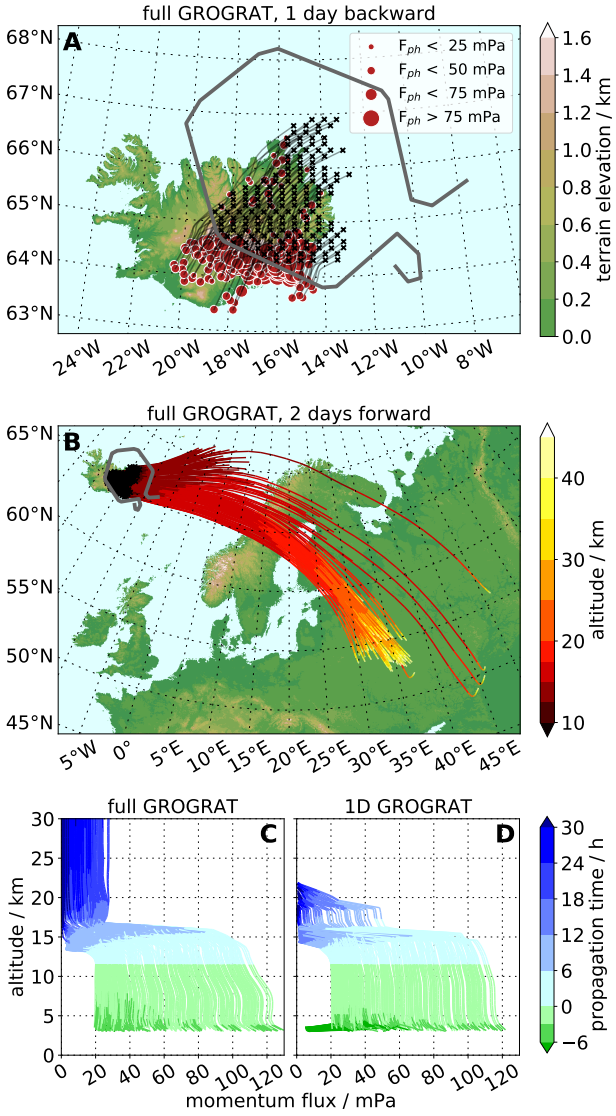


**Figure 7.** Ray traces calculated using the GROGRAT model. The starting positions of the rays are marked with black crosses and the grey line indicates the flight path. The size of the red circles in A indicates the GWMF at the end of the ray. Panel A shows the backward ray traces and panel B the forward ray traces, all starting at the measurement locations. Panels C and D show the change of GWMF with height for a full 4D GROGRAT (C) model run and a solely vertical 1D run (D).

horizontally more than 2000 km (Fig. 7B). Over Eastern Europe, the GWs are refracted due to a horizontal wind shear and, thus, change their horizontal wave vector from southward to westward. This allows the waves to quickly propagate upward into the westerly wind in the mid stratosphere. ~~In the wind shear below 20 km, the horizontal wave vectors turn from southward to westward, which then allows for a quick upward propagation into the westerly wind in the mid stratosphere.~~ (RC2: #43)

To mimic a typical GW parameterization scheme used in GCMs (McLandress, 1998), a second GROGRAT run (1D-GROGRAT) was performed with solely vertical propagation, time-independent background, and a horizontal wave direction constant with respect to altitude. In contrast to the full GROGRAT version (Fig. 7C), where the GWs propagate into the mid stratosphere, the GWs in the simplified version dissipate below 20 km (Fig. 7D). Two processes might play a significant role here: First, in the 1D GROGRAT version the GWs are not refracted and the wave vectors do not change its horizontal orientation with altitude. The westerly background winds at higher altitudes do not favor the propagation of GWs with wave vectors perpendicular to the wind direction. Second, in the full GROGRAT run, the GWs propagate horizontally away from the source. Hence, the GWs avoid the critical level positioned above the source location and more GWMF is transported to higher altitudes. Global mountain wave modeling (Xu et al., 2017) suggests that this effect may prevail also on a global basis. (RC2: #44)

Neither a realistic orientation of the wave vector, nor oblique GW propagation are incorporated in GW parameterizations used in current climate and weather prediction models (McLandress, 1998; Alexander and Dunkerton, 1999; Richter et al., 2010; McLandress et al., 2012; Garcia et al., 2017). However, both processes are context of several studies aiming to improve GW parameterizations (Preusse et al., 2009; Sato et al., 2009; Kalisch et al., 2014; Amemiya and Sato, 2016; Ribstein and Achatz, 2016; Garcia et al., 2017). The present paper provides a strong motivation to finally implement these processes in current climate and weather prediction models. Especially, as this could close gaps of GWMF in regions with sparse sources (McLandress et al., 2012) and reduce the cold-pole bias of climate and weather prediction models in the lower stratosphere (Garcia et al., 2017). ~~Accordingly, the degree to which GW propagation is simplified determines the location and altitude at which GWMF is deposited. This is also very important for climate and weather prediction models, which often have difficulties in applying the drag of dissipating GWs at the correct altitude and location (McLandress et al., 2012). The importance of oblique propagation highlighted here corroborates results of several model studies (Sato et al., 2009; Preusse et al., 2009; Kalisch et al., 2014; Ribstein and Achatz, 2016) and could close gaps of GWMF in regions with sparse sources (McLandress et al., 2012).~~ (RC2: #44)

## 4 Conclusions

In this paper, we presented the first tomographic measurements of temperature perturbations induced by a GW event. The 3D measurements recorded by GLORIA, the first airborne implementation of a novel limb imaging technique, enabled the deduction of direction-resolved GWMF and the identification of two distinct wave packets. The retrieved 3D wave vectors were used as input in the ray-tracing model GROGRAT, which highlighted the orography of Iceland as the most likely GW source. Furthermore, upward from 11 km the wave packets propagate obliquely as is seen from the observation and reproduced by the ray-tracer. A comparison between the full GROGRAT model and a simplified 1D version indicated the relevance of oblique propagation for the GWMF deposition height. In the simplified version, all GWs deposited their momentum at an altitude of around 20 km, whereas in the full version, waves were able to vertically propagate to the top of the model at 45 km and horizontally more than 2000 km away from their source, thus redistributing GWMF significantly. Given that weather

prediction and climate models routinely use 1D models of GW propagation, the present findings demonstrate that considering 3D propagation could lead to significant improvements in weather forecasting and climate prediction.

*Data availability.* The tomographic retrieval data is available on the HALO database (https://halo-db.pa.op.dlr.de/).

*Competing interests.* The authors declare that they have no conflict of interest.

*Acknowledgements.* This work was partly supported by the Bundesministerium für Bildung und Forschung (BMBF) under project 01LG1206C (ROMIC/GW-LCYCLE), as well as by the European Space Agency (ESA) under contract 4000115111/15/NL/FF/ah (GWEX) and the Deutsche Forschungsgemeinschaft (DFG) project PR 919/4-1 (MS-GWaves/SV), which is part of the DFG researchers group FOR 1898 (MS-GWaves). The retrievals were performed on the JURECA supercomputer at the Jülich Supercomputing Center (JSC) as part of the JIEK72 project. The results are based on the efforts of all members of the GLORIA team, including the technology institutes ZEA-1 and ZEA-2 at Forschungszentrum Jülich and the Institute for Data Processing and Electronics at the Karlsruhe Institute of Technology. We would also like to thank the pilots and ground-support team at the Flight Experiments facility of the Deutsches Zentrum für Luft- und Raumfahrt (DLR-FX). Special thanks go to Andreas Diez at DLR-FX for providing the in-situ temperature data shown in Fig. 4 and to Corwin Wright at the Centre for Space, Atmospheric and Oceanic Science at University of Bath for providing the plotting code for Fig. 2.

## References


Alexander, M. J. and Dunkerton, T. J.: A Spectral Parameterization of Mean-Flow Forcing due to Breaking Gravity Waves, Journal of the Atmospheric Sciences, 56, 4167–4182, doi:10.1175/1520-0469(1999)056<4167:ASPOMF>2.0.CO;2, 1999.

Alexander, M. J. and Pfister, L.: Gravity wave momentum flux in the lower stratosphere over convection, Geophys. Res. Lett., 22, 2029–2032, doi:10.1029/95GL01984, 1995.

Alexander, M. J. and Rosenlof, K. H.: Gravity-wave forcing in the stratosphere: Observational constraints from the Upper Atmosphere Research Satellite and implications for parameterization in global models, Geophys. Res. Lett., 108, doi:10.1029/2003JD003373, 2003.

Alexander, M. J., Geller, M., McLandress, C., Polavarapu, S., Preusse, P., Sassi, F., Sato, K., Eckermann, S., Ern, M., Hertzog, A., Kawatani, Y., Pulido, M., Shaw, T. A., Sigmond, M., Vincent, R., and Watanabe, S.: Recent developments in gravity-wave effects in climate models and the global distribution of gravity-wave momentum flux from observations and models, Q. J. R. Meteorol. Soc., 136, 1103–1124, doi:10.1002/qj.637, 2010.

Amemiya, A. and Sato, K.: A New Gravity Wave Parameterization Including Three-Dimensional Propagation, Journal of the Meteorological Society of Japan. Ser. II, advpub, doi:10.2151/jmsj.2016-013, 2016.

Beres, J. H., Garcia, R. R., Boville, B. A., and Sassi, F.: Implementation of a gravity wave source spectrum parameterization dependent on the properties of convection in the Whole Atmosphere Community Climate Model (WACCM), Journal of Geophysical Research: Atmospheres, 110, doi:10.1029/2004JD005504, http://dx.doi.org/10.1029/2004JD005504, d10108, 2005.

Boccara, G., Hertzog, A., Vincent, R. A., and Vial, F.: Estimation of gravity wave momentum flux and phase speeds from quasi-Lagrangian stratospheric balloon flights. Part I: Theory and simulations, J. Atmos. Sci., 65, 3042–3055, doi:10.1175/2008JAS2709.1, 2008.

Bossert, K., Fritts, D. C., Pautet, P.-D., Williams, B. P., Taylor, M. J., Kaifler, B., Dörnbrack, A., Reid, I. M., Murphy, D. J., Spargo, A. J., and MacKinnon, A. D.: Momentum flux estimates accompanying multiscale gravity waves over Mount Cook, New Zealand, on 13 July 2014 during the DEEPWAVE campaign, J. Geophys. Res. Atmos., 120, 9323–9337, doi:10.1002/2015JD023197, http://dx.doi.org/10.1002/2015JD023197, 2015JD023197, 2015.

Bushell, A. C., Butchart, N., Derbyshire, S. H., Jackson, D. R., Shutts, G. J., Vosper, S. B., and Webster, S.: Parameterized Gravity Wave Momentum Fluxes from Sources Related to Convection and Large-Scale Precipitation Processes in a Global Atmosphere Model, J. Atmos. Sci., 72, 4349–4371, doi:10.1175/JAS-D-15-0022.1, 2015.

Butchart, N.: The Brewer-Dobson circulation, Reviews of Geophysics, 52, 157–184, doi:10.1002/2013RG000448, http://dx.doi.org/10.1002/2013RG000448, 2014.

Cao, B., Heale, C. J., Guo, Y., Liu, A. Z., and Snively, J. B.: Observation and modeling of gravity wave propagation through reflection and critical layers above Andes Lidar Observatory at Cerro Pachón, Chile, J. Geophys. Res. Atmos., 121, 12,737–12,750, doi:10.1002/2016JD025173, http://dx.doi.org/10.1002/2016JD025173, 2016JD025173, 2016.

de la Camara, A. and Lott, F.: A parameterization of gravity waves emitted by fronts and jets, Geophys. Res. Lett., 42, 2071–2078, doi:10.1002/2015GL063298, 2015.

Dunkerton, T.: The role of gravity waves in the quasi-biennial oscillation, J. Geophys. Res., 102, 26 053–26 076, doi:10.1029/96JD02999, 1997.

Eckermann, S. D. and Vincent, R. A.: Falling sphere observations of anisotropic gravity wave motions in the upper stratosphere over Australia, Pure Appl. Geophys., 130, 509–532, 1989.

Ern, M., Preusse, P., Alexander, M. J., and Warner, C. D.: Absolute values of gravity wave momentum flux derived from satellite data, Journal of Geophysical Research: Atmospheres, 109, doi:10.1029/2004JD004752, http://dx.doi.org/10.1029/2004JD004752, 2004.

Ern, M., Ploeger, F., Preusse, P., Gille, J. C., Gray, L. J., Kalisch, S., Mlynczak, M. G., Russell III, J. M., and Riese, M.: Interaction of gravity waves with the QBO: A satellite perspective, Journal of Geophysical Research: Atmospheres, 119, 2329–2355, doi:10.1002/2013JD020731, 2014.

Ern, M., Trinh, Q. T., Kaufmann, M., Krisch, I., Preusse, P., Ungermann, J., Zhu, Y., Gille, J. C., Mlynczak, M. G., Russell, III, J. M., Schwartz, M. J., and Riese, M.: Satellite observations of middle atmosphere gravity wave absolute momentum flux and of its vertical gradient during recent stratospheric warmings, Atmos. Chem. Phys., 16, 9983–10 019, doi:10.5194/acp-16-9983-2016, 2016.

Ern, M., Hoffmann, L., and Preusse, P.: Directional gravity wave momentum fluxes in the stratosphere derived from high-resolution AIRS temperature data, Geophys. Res. Lett., 44, 475–485, doi:10.1002/2016GL072007, 2017.

Friedl-Vallon, F., Gulde, T., Hase, F., Kleinert, A., Kulessa, T., Maucher, G., Neubert, T., Olschewski, F., Piesch, C., Preusse, P., Rongen, H., Sartorius, C., Schneider, H., Schönfeld, A., Tan, V., Bayer, N., Blank, J., Dapp, R., Ebersoldt, A., Fischer, H., Graf, F., Guggenmoser, T., Höpfner, M., Kaufmann, M., Kretschmer, E., Latzko, T., Nordmeyer, H., Oelhaf, H., Orphal, J., Riese, M., Schardt, G., Schillings, J., Sha, M. K., Suminska-Ebersoldt, O., and Ungermann, J.: Instrument concept of the imaging Fourier transform spectrometer GLORIA, Atmos. Meas. Tech., 7, 3565–3577, doi:10.5194/amt-7-3565-2014, 2014.

Fritts, D. C. and Alexander, M. J.: Gravity wave dynamics and effects in the middle atmosphere, Rev. Geophys., 41, doi:10.1029/2001RG000106, 2003.

Fritts, D. C., Smith, R. B., Taylor, M. J., Doyle, J. D., Eckermann, S. D., Doernbrack, A., Rapp, M., Williams, B. P., Pautet, P. D., Bossert, K., Criddle, N. R., Reynolds, C. A., Reinecke, P. A., Uddstrom, M., Revell, M. J., Turner, R., Kaifler, B., Wagner, J. S., Mixa, T., Kruse, C. G., Nugent, A. D., Watson, C. D., Gisinger, S., Smith, S. M., Lieberman, R. S., Laughman, B., Moore, J. J., Brown, W. O., Haggerty, J. A., Rockwell, A., Stossmeister, G. J., Williams, S. F., Hernandez, G., Murphy, D. J., Klekociuk, A. R., Reid, I. M., and Ma, J.: The Deep Propagating Gravity Wave Experiment (DEEPWAVE): An Airborne and Ground-Based Exploration of Gravity Wave Propagation and Effects from Their Sources throughout the Lower and Middle Atmosphere, Bull. Amer. Meteorol. Soc., 97, 425–453, doi:10.1175/BAMS-D-14-00269.1, 2016.

Garcia, R. R., Smith, A. K., Kinnison, D. E., de la Camara, A., and Murphy, D. J.: Modification of the Gravity Wave Parameterization in the Whole Atmosphere Community Climate Model: Motivation and Results, J. Atmos. Sci., 74, 275–291, doi:10.1175/JAS-D-16-0104.1, 2017.

Geller, M. A., Alexander, M. J., Love, P. T., Bacmeister, J., Ern, M., Hertzog, A., Manzini, E., Preusse, P., Sato, K., Scaife, A. A., and Zhou, T.: A comparison between gravity wave momentum fluxes in observations and climate models, J. Clim., 26, 6383–6405, doi:10.1175/JCLI-D-12-00545.1, 2013.

Gerrard, A. J., Kane, T. J., Eckermann, S. D., and Thayer, J. P.: Gravity waves and mesospheric clouds in the summer middle atmosphere: A comparison of lidar measurements and ray modeling of gravity waves over Sonderstrom, Greenland, J. Geophys. Res., 109, doi:10.1029/2002JD002783, 2004.

Guest, F., Reeder, M., Marks, C., and Karoly, D.: Inertia-gravity waves observed in the lower stratosphere over Macquarie Island, J. Atmos. Sci., 57, 737–752, 2000.

Hertzog, A., Boccara, G., Vincent, R. A., Vial, F., and Coquerez, P.: Estimation of gravity-wave momentum flux and phase speeds from long-duration stratospheric balloon flights. 2: Results from the Vorcore campaign in Antarctica, J. Atmos. Sci., 65, 3056–3070, doi:10.1175/2008JAS2710.1, 2008.

Hertzog, A., Alexander, M. J., and Plougonven, R.: On the Intermittency of Gravity Wave Momentum Flux in the Stratosphere, Journal of the Atmospheric Sciences, 69, 3433–3448, doi:10.1175/JAS-D-12-09.1, https://doi.org/10.1175/JAS-D-12-09.1, 2012.

Hines, C. O.: Doppler-spread parameterization of gravity-wave momentum deposition in the middle atmosphere. Part 1: Basic formulation, Journal of Atmospheric and Solar-Terrestrial Physics, 59, 371 – 386, doi:https://doi.org/10.1016/S1364-6826(96)00079-X, http://www.sciencedirect.com/science/article/pii/S136468269600079X, 1997.

Holton, J. R.: The role of gravity wave induced drag and diffusion on the momentum budget of the mesosphere, J. Atmos. Sci., 39, 791–799, 1982.

Holton, J. R.: The Influence of Gravity Wave Breaking on the General Circulation of the Middle Atmosphere, Journal of the Atmospheric Sciences, 40, 2497–2507, doi:10.1175/1520-0469(1983)040<2497:TIOGWB>2.0.CO;2, 1983.

Kalisch, S., Preusse, P., Ern, M., Eckermann, S. D., and Riese, M.: Differences in gravity wave drag between realistic oblique and assumed vertical propagation, Journal of Geophysical Research: Atmospheres, 119, 10,081–10,099, doi:10.1002/2014JD021779, 2014.

Kaufmann, M., Blank, J., Guggenmoser, T., Ungermann, J., Engel, A., Ern, M., Friedl-Vallon, F., Gerber, D., Grooß, J. U., Guenther, G., Höpfner, M., Kleinert, A., Kretschmer, E., Latzko, T., Maucher, G., Neubert, T., Nordmeyer, H., Oelhaf, H., Olschewski, F., Orphal, J., Preusse, P., Schlager, H., Schneider, H., Schuettemeyer, D., Stroh, F., Suminska-Ebersoldt, O., Vogel, B., M. Volk, C., Woiwode, W., and Riese, M.: Retrieval of three-dimensional small-scale structures in upper-tropospheric/lower-stratospheric composition as measured by GLORIA, Atmos. Meas. Tech., 8, 81–95, doi:10.5194/amt-8-81-2015, http://www.atmos-meas-tech.net/8/81/2015/, 2015.

Kawatani, Y., Sato, K., Dunkerton, T. J., Watanabe, S., Miyahara, S., and Takahashi, M.: The roles of equatorial trapped waves and three-dimensionally propagating gravity waves in driving the quasibiennial oscillation. Part I: zonal mean wave forcing, J. Atmos. Sci., 67, 963–980, doi:10.1175/2009JAS3222.1, 2010.

Kidston, J., Scaife, A. A., Hardiman, S. C., Mitchell, D. M., Butchart, N., Baldwin, M. P., and Gray, L. J.: Stratospheric influence on tropospheric jet streams, storm tracks and surface weather, Nature Geoscience, 8, 433–440, doi:10.1038/ngeo2424, 2015.

Kim, Y. H., Bushell, A. C., Jackson, D. R., and Chun, H. Y.: Impacts of introducing a convective gravity-wave parameterization upon the QBO in the Met Office Unified Model, Geophys. Res. Lett., 40, 1873–1877, doi:10.1002/grl.50353, 2013.

Lehmann, C. I., Kim, Y.-H., Preusse, P., Chun, H.-Y., Ern, M., and Kim, S.-Y.: Consistency between Fourier transform and small-volume few-wave decomposition for spectral and spatial variability of gravity waves above a typhoon, Atmospheric Measurement Techniques, 5, 1637–1651, doi:10.5194/amt-5-1637-2012, http://www.atmos-meas-tech.net/5/1637/2012/, 2012.

Lu, X., Chen, C., Huang, W., Smith, J. A., Chu, X., Yuan, T., Pautet, P.-D., Taylor, M. J., Jie, G., and Cullens, C. Y.: A coordinated study of 1 h mesoscale gravity waves propagating from Logan to Boulder with CRRL Na Doppler lidars and temperature mapper, J. Geophys. Res. Atmos., 120, 10,006–10,021, doi:10.1002/2015JD023604, http://dx.doi.org/10.1002/2015JD023604, 2015JD023604, 2015.

Marks, C. J. and Eckermann, S. D.: A Three-Dimensional Nonhydrostatic Ray-Tracing Model for Gravity Waves: Formulation and Preliminary Results for the Middle Atmosphere, J. Atmos. Sci., 52, 1959–1984, doi:10.1175/1520-0469(1995)052<1959:ATDNRT>2.0.CO;2, 1995.

McFarlane, N.: The Effect of Orographically Excited Gravity Wave Drag on the General Circulation of the Lower Stratosphere and Troposphere, J. Atmos. Sci., 44, 1775–1800, 1987.

McLandress, C.: On the importance of gravity waves in the middle atmosphere and their parameterization in general circulation models, J. Atm. Sol.-Terr. Phys., 60, 1357–1383, doi:10.1016/S1364-6826(98)00061-3, 1998.

McLandress, C., Shepherd, T. G., Polavarapu, S., and Beagley, S. R.: Is Missing Orographic Gravity Wave Drag near 60°S the Cause of the Stratospheric Zonal Wind Biases in Chemistry-Climate Models?, J. Atmos. Sci., 69, 802–818, doi:10.1175/JAS-D-11-0159.1, http://dx.doi.org/10.1175/JAS-D-11-0159.1, 2012.

Podglajen, A., Hertzog, A., Plougonven, R., and Legras, B.: Lagrangian temperature and vertical velocity fluctuations due to gravity waves in the lower stratosphere, Geophys. Res. Lett., 43, 3543–3553, doi:10.1002/2016GL068148, 2016.

Pramitha, M., Venkat Ratnam, M., Taori, A., Krishna Murthy, B. V., Pallamraju, D., and Vijaya Bhaskar Rao, S.: Evidence for tropospheric wind shear excitation of high-phase-speed gravity waves reaching the mesosphere using the ray-tracing technique, Atmos. Chem. Phys., 15, 2709–2721, doi:10.5194/acp-15-2709-2015, 2015.

Preusse, P., Eckermann, S. D., Ern, M., Oberheide, J., Picard, R. H., Roble, R. G., Riese, M., Russell III, J. M., and Mlynczak, M. G.: Global ray tracing simulations of the SABER gravity wave climatology, J. Geophys. Res. Atmos., 114, doi:10.1029/2008JD011214, 2009.

Preusse, P., Ern, M., Bechtold, P., Eckermann, S. D., Kalisch, S., Trinh, Q. T., , and Riese, M.: Characteristics of gravity waves resolved by ECMWF, Atmos. Chem. Phys., 14, 10 483–10 508, doi:10.5194/acp-14-10483-2014, 2014.

Ribstein, B. and Achatz, U.: The interaction between gravity waves and solar tides in a linear tidal model with a 4-D ray-tracing gravity-wave parameterization, Journal of Geophysical Research: Space Physics, 121, 8936–8950, doi:10.1002/2016JA022478, http://dx.doi.org/10.1002/2016JA022478, 2016JA022478, 2016.

Richter, J. H., Sassi, F., and Garcia, R. R.: Toward a Physically Based Gravity Wave Source Parameterization in a General Circulation Model, Journal of the Atmospheric Sciences, 67, 136–156, doi:10.1175/2009JAS3112.1, 2010.

Riese, M., Spang, R., Preusse, P., Ern, M., Jarisch, M., Offermann, D., and Grossmann, K. U.: Cryogenic Infrared Spectrometers and Telescopes for the Atmosphere (CRISTA) data processing and atmospheric temperature and trace gas retrieval, J. Geophys. Res. Atmos., 104, 16 349–16 367, doi:10.1029/1998JD100057, http://dx.doi.org/10.1029/1998JD100057, 1999.

Riese, M., Oelhaf, H., Preusse, P., Blank, J., Ern, M., Friedl-Vallon, F., Fischer, H., Guggenmoser, T., Höpfner, M., Hoor, P., Kaufmann, M., Orphal, J., Plöger, F., Spang, R., Suminska-Ebersoldt, O., Ungermann, J., Vogel, B., and Woiwode, W.: Gimballed Limb Observer for Radiance Imaging of the Atmosphere (GLORIA) scientific objectives, Atmos. Meas. Tech., 7, 1915–1928, doi:10.5194/amt-7-1915-2014, 2014.

Sandu, I., Bechtold, P., Beljaars, A., Bozzo, A., Pithan, F., Shepherd, T. G., and Zadra, A.: Impacts of parameterized orographic drag on the Northern Hemisphere winter circulation, J. Adv. Model. Earth Syst., 8, 196–211, doi:10.1002/2015MS000564, 2016.

Sato, K., Watanabe, S., Kawatani, Y., Tomikawa, Y., Miyazaki, K., and Takahashi, M.: On the origins of mesospheric gravity waves, Geophys. Res. Lett., 36, doi:10.1029/2009GL039908, 2009.

Savitzky, A. and Golay, M. J. E.: Smoothing and Differentiation of Data by Simplified Least Squares Procedures., Analytical Chemistry, 36, 1627–1639, doi:10.1021/ac60214a047, http://dx.doi.org/10.1021/ac60214a047, 1964.

Scaife, A. A., Karpechko, A. Y., Baldwin, M. P., Brookshaw, A., Butler, A. H., Eade, R., Gordon, M., MacLachlan, C., Martin, N., Dunstone, N., and Smith, D.: Seasonal winter forecasts and the stratosphere, Atmospheric Science Letters, 17, 51–56, doi:10.1002/asl.598, http://dx.doi.org/10.1002/asl.598, 2016.

Scinocca, J. F. and McFarlane, N. A.: The parametrization of drag induced by stratified flow over anisotropic orography, Quarterly Journal of the Royal Meteorological Society, 126, 2353–2393, doi:10.1002/qj.49712656802, http://dx.doi.org/10.1002/qj.49712656802, 2000.

Sigmond, M. and Scinocca, J. F.: The Influence of the Basic State on the Northern Hemisphere Circulation Response to Climate Change, J. Clim., 23, 1434–1446, doi:10.1175/2009JCLI3167.1, 2010.

Siskind, D. E.: Simulations of the winter stratopause and summer mesopause at varying spatial resolutions, J. Geophys. Res. Atmos., 119, 461–470, doi:10.1002/2013JD020985, 2014.

Smith, R. B., Nugent, A. D., Kruse, C. G., Fritts, D. C., Doyle, J. D., Eckermann, S. D., Taylor, M. J., Doernbrack, A., Uddstrom, M., Cooper, W., Romashkin, P., Jensen, J., and Beaton, S.: Stratospheric Gravity Wave Fluxes and Scales during DEEPWAVE, J. Atmos. Sci., 73, 2851–2869, doi:10.1175/JAS-D-15-0324.1, 2016.

Stober, G., Sommer, S., Rapp, M., and Latteck, R.: Investigation of gravity waves using horizontally resolved radial velocity measurements, Atmos. Meas. Tech., 6, 2893–2905, doi:10.5194/amt-6-2893-2013, http://www.atmos-meas-tech.net/6/2893/2013/, 2013.

Ungermann, J., Kaufmann, M., Hoffmann, L., Preusse, P., Oelhaf, H., Friedl-Vallon, F., and Riese, M.: Towards a 3-D tomographic retrieval for the air-borne limb-imager GLORIA, Atmos. Meas. Tech., 3, 1647–1665, doi:10.5194/amt-3-1647-2010, 2010.

Ungermann, J., Blank, J., Lotz, J., Leppkes, K., Hoffmann, L., Guggenmoser, T., Kaufmann, M., Preusse, P., Naumann, U., and Riese, M.: A 3-D tomographic retrieval approach with advection compensation for the air-borne limb-imager GLORIA, Atmos. Meas. Tech., 4, 2509–2529, doi:10.5194/amt-4-2509-2011, 2011.

Ungermann, J., Blank, J., Dick, M., Ebersoldt, A., Friedl-Vallon, F., Giez, A., Guggenmoser, T., Höpfner, M., Jurkat, T., Kaufmann, M., Kaufmann, S., Kleinert, A., Krämer, M., Latzko, T., Oelhaf, H., Olchewski, F., Preusse, P., Rolf, C., Schillings, J., Suminska-Ebersoldt, O., Tan, V., Thomas, N., Voigt, C., Zahn, A., Zöger, M., and Riese, M.: Level 2 processing for the imaging Fourier transform spectrometer GLORIA: derivation and validation of temperature and trace gas volume mixing ratios from calibrated dynamics mode spectra, Atmos. Meas. Tech., 8, 2473–2489, doi:10.5194/amt-8-2473-2015, 2015.

Wagner, J., Doernbrack, A., Rapp, M., Gisinger, S., Ehard, B., Bramberger, M., Witschas, B., Chouza, F., Rahm, S., Mallaun, C., Baumgarten, G., and Hoor, P.: Observed versus simulated mountain waves over Scandinavia-improvement of vertical winds, energy and momentum fluxes by enhanced model resolution?, Atmos. Chem. Phys., 17, 4031–4052, doi:10.5194/acp-17-4031-2017, 2017.

Wang, L. and Geller, M. A.: Morphology of gravity-wave energy as observed from 4 years (1998-2001) of high vertical resolution U.S. radiosonde data, J. Geophys. Res., 108, doi:10.1029/2002JD002786, 2003.

Wright, C. J., Hindley, N. P., Hoffmann, L., Alexander, M. J., and Mitchell, N. J.: Exploring gravity wave characteristics in 3-D using a novel S-transform technique: AIRS/Aqua measurements over the Southern Andes and Drake Passage, Atmos. Chem. Phys., 17, 8553–8575, doi:10.5194/acp-17-8553-2017, https://www.atmos-chem-phys.net/17/8553/2017/, 2017.

Xu, X., Wang, Y., Xue, M., and Zhu, K.: Impacts of Horizontal Propagation of Orographic Gravity Waves on the Wave Drag in the Stratosphere and Lower Mesosphere, J. Geophys. Res. Atmos., doi:10.1002/2017JD027528, http://dx.doi.org/10.1002/2017JD027528, 2017JD027528, 2017.

Zhang, S. D., Huang, C. M., Huang, K. M., Yi, F., Zhang, Y. H., Gong, Y., and Gan, Q.: Spatial and seasonal variability of medium- and high-frequency gravity waves in the lower atmosphere revealed by US radiosonde data, Ann. Geophys., 32, 1129–1143, doi:10.5194/angeo-32-1129-2014, 2014.

## Appendix A: Error analysis

In this section the effects of different errors onto the ray-tracing results presented in Section 3.2 are discussed. These errors may, in principle, be caused during each of the three main processing steps: temperature retrieval, background removal and sinusoidal wave fits (S3D). Retrieval errors can be divided into precision and accuracy (cf. Section 2.1). Due to the high number of independent data in each S3D cube, the precision error (mainly due to noise) can be neglected, in particular since in this paper only GW events with amplitudes above a threshold of 0.5 K are considered. The error sources which lead to the accuracy error are systematic and slowly varying. Thus, their impact is mostly mitigated by the background removal.

The background removal separates the data into large scale variations and short scale fluctuations, the latter interpreted as GWs. The main effect of an unfavorably tuned background removal would be to eliminate real GWs. However, it would not introduce errors in the fitted wave vectors. Thus, this has to be considered in a comparison with other data, but is not included in the further error discussion.

The third step, the S3D method, is based on the assumption that the fitting volume is filled by a homogeneous wave with a constant wave amplitude and a constant wave vector over the fitting volume. The discussion in sections 2.2 and 3.1 demonstrates that this assumption is only valid to a certain degree. In particular, we notice that the direction of the horizontal wave vector and the vertical wavelength change with height as the wave is refracted by a changing background wind.

We use the results of the ray-tracer to estimate errors due to this change over height within the fitting volume. In Fig. A1 left column the instantaneous value $\xi_{z=11.5}$ of the ray at the middle point of each fitting volume is compared to an average $\bar{\xi}$ of all values of the ray in the height range of the respective S3D fitting volume~~In Fig. A1 left column the instantaneous value $\xi_{z=11.5}$ at the middle point of the fitting volume of each individual ray is compared to an average value $\bar{\xi}$ over the full height range of the S3D fitting volume~~ (RC1: #4) (comparable to the S3D fitting result); here $\xi$ stands for either the vertical or horizontal wavelength or the horizontal wave direction. The mean vertical wavelength shows a systematic low bias of around $10\%$ compared to the instantaneous value in the middle (Fig. A1 A). This effect is taken into account and all vertical wavelengths from the sinusoidal fit (Section 3.1) are scaled with a factor of 1.1 before being used in the ray-tracing analysis (Section 3.2). For the horizontal wavelength (Fig. A1 C) and the horizontal wave direction (Fig. A1 E) no systematic bias could be identified.

As mentioned before, the accuracy with which the input wave parameters $\xi$ are determined is of high importance. This is highlighted through varying the values $\xi$ by factor $\epsilon_\xi$ and comparing the ray-tracing results with a reference run. The variations $\epsilon_\xi$ for the vertical wavelength and the horizontal wave direction are chosen to be half the difference of the wave parameters at the upper ($\xi_{z=max}$) and lower ($\xi_{z=min}$) boundary of the S3D fitting volume as determined by the ray-tracing reference run (Fig. A1 B, F). The horizontal wavelength does not change much over the height of the fitting volume (Fig. A1 D). However Fig. 3 and Fig. 5 indicate a significant variation of the horizontal wavelength over the horizontal extent of the fitting volume. Hence, for the error estimate ray-tracing calculations we chose an error value of $\pm 15\%$ as estimate for the horizontal variation of the horizontal wavelength within the S3D fitting volume. In Tab. A1 the used error estimates for the three wave parameters are summarized.

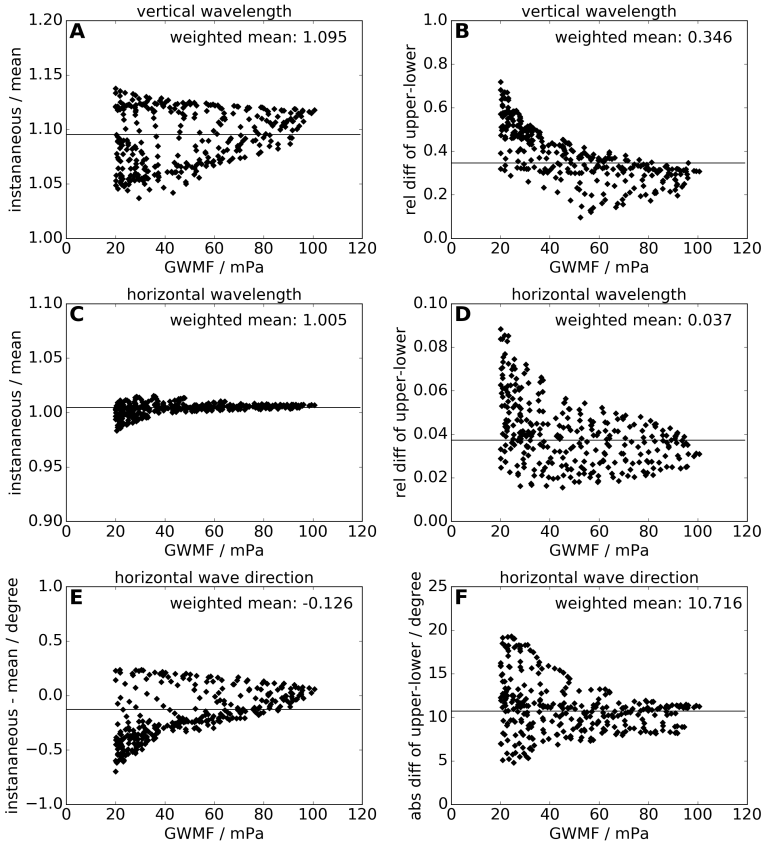


**Figure A1.** Comparison of mean values over the whole S3D fitting volume and instantaneous values in the middle for different wave parameters (left column) and variation of wave parameters from the lower to the upper boundary of the S3D fitting volume (right column). For all graphs GWMF weighted means are calculated and depicted as black lines.

**Table A1.** Error estimates for the wave parameters inferred by the S3D method based on the change of the parameters over the extent of the fitting cube.

| | |
|---|---|
| error estimate of the vertical wavelength | $\pm 17\%$ |
| error estimate of the horizontal wavelength | $\pm 15\%$ |
| error estimate of the horizontal wave direction | $\pm 5.5^{\circ}$ |

The results of the back-tracing runs with wave parameters varied by the error estimates in Tab. A1 are shown in Fig. A2. Longer vertical wavelengths (Fig. A2 C-D) lead to more northward located sources, while rays from shorter vertical wavelengths (Fig. A2 B) end southward, i.e. upstream of Iceland over the ocean. This is due to the fact, that longer vertical wavelengths are associated with higher horizontal phase velocities and hence higher horizontal group velocities. Accordingly, in the case of shorter vertical wavelengths the waves are not able to compensate the background wind velocity and would origin from

an upstream source. Actually, we find that the inferred bias (10% larger values for the vertical wavelengths), when corrected, improves the match of the ray-positions with the topography (Fig. A2 C).

The horizontal wave direction has similar impact: When the wave is turned more into the south-easterly background flow (Fig. A2 H) the ray-paths are more vertically oriented and therefore reach the ground closer to the measurement volume. When they are turned away from the background wind (Figure A2 G), the intrinsic group velocity and the background wind are at an angle, the intrinsic group velocity does not fully compensate the background wind, and the waves cover a larger horizontal distance reaching onto the ocean upstream of Iceland.

Similar variations for the forward ray-traces are shown in Fig. A3. In all cases except for shorter vertical wavelengths, a major group of ray-traces reaches the model top at 45km altitude (white dots), i.e. our main findings presented in Sec. 3.2 are robust.

The error estimates demonstrate that a correct identification of the GW source is only feasible for highly accurate wave characterization, such as achieved here thanks to the high spatial resolution and accuracy of GLORIA 3D temperature measurements.

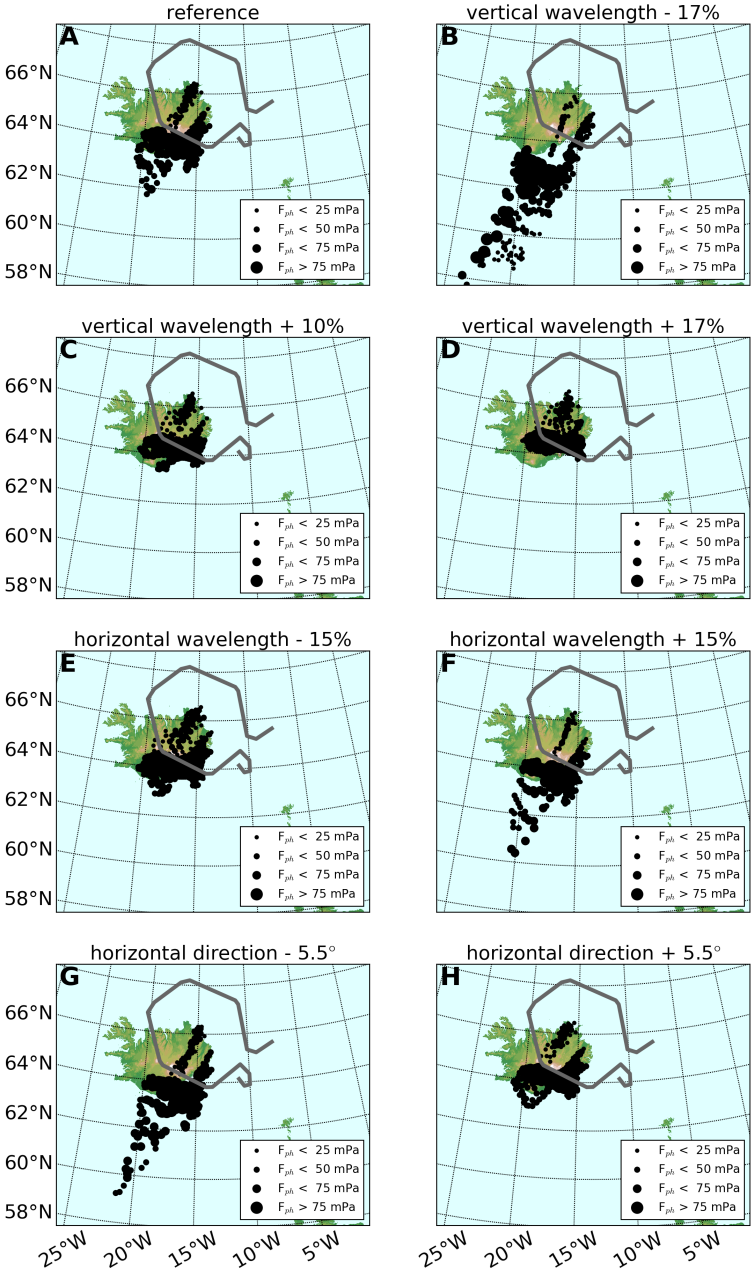


**Figure A2.** Backward ray-tracing with varying input wave parameters. The black dots mark the ray positions at 3 km altitude.

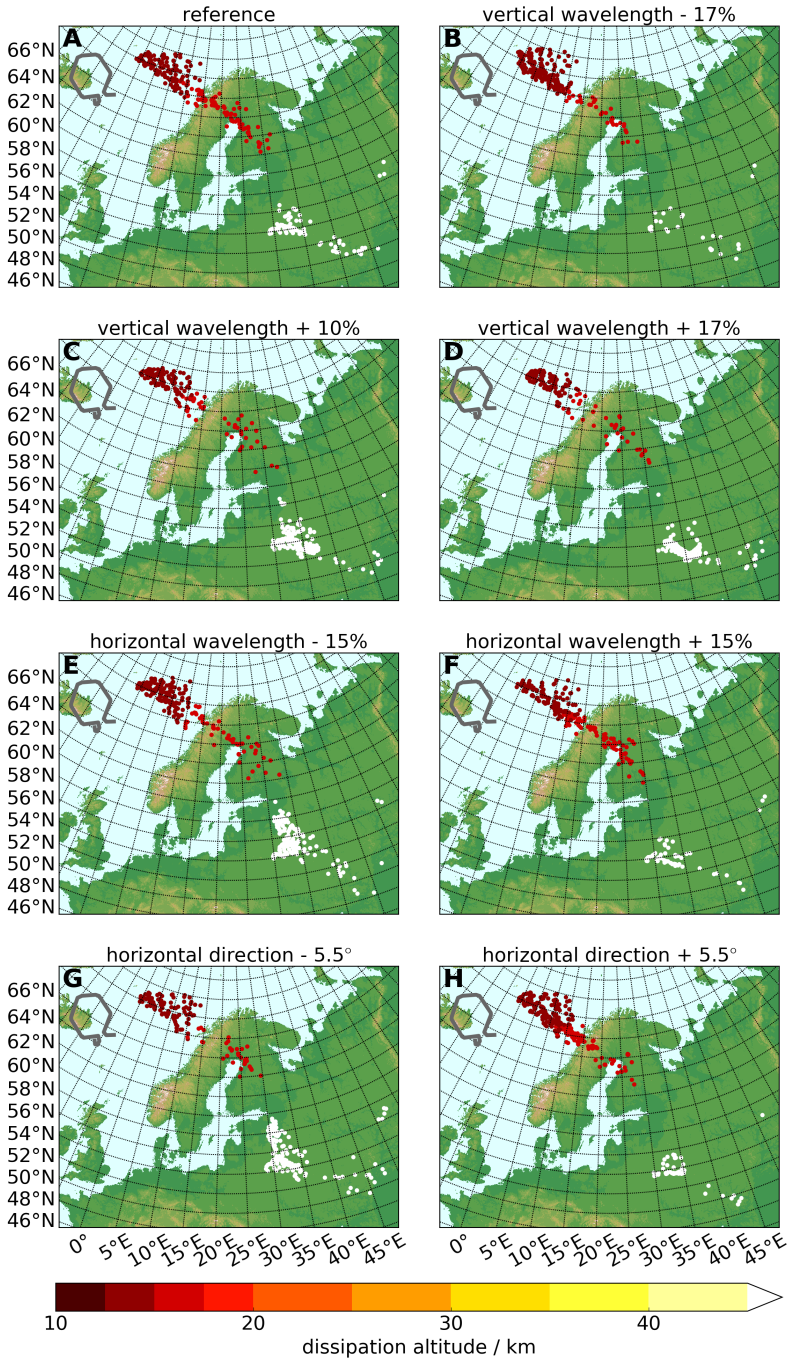


**Figure A3.** Forward ray-tracing with varying input wave parameters. The dots mark the dissipation point of the ray, the colour indicates the dissipation height. White dots mark waves which reach the model top at 45 km altitude.